ARCHIVIO ISTITUZIONALE
DELLA RICERCA

Alma Mater Studiorum Università di Bologna
Archivio istituzionale della ricerca

Output-only damage diagnosis for plan-symmetric buildings with asymmetric damage using modal flexibility-based deflections

This is the final peer-reviewed author's accepted manuscript (postprint) of the following publication:

Published Version:
Bernagozzi, G., Ventura, C.E., Allahdadian, S., Kaya, Y., Landi, L., Diotallevi, P.P. (2020). Output-only damage diagnosis for plan-symmetric buildings with asymmetric damage using modal flexibility-based deflections. ENGINEERING STRUCTURES, 207, 1-27 [10.1016/j.engstruct.2019.110015].

Availability:
This version is available at: https://hdl.handle.net/11585/733239 since: 2020-03-26

Published:

DOI: http://doi.org/10.1016/j.engstruct.2019.110015

Terms of use:

Some rights reserved. The terms and conditions for the reuse of this version of the manuscript are specified in the publishing policy. For all terms of use and more information see the publisher's website.

This item was downloaded from IRIS Università di Bologna (https://cris.unibo.it/).
When citing, please refer to the published version.

(Article begins on next page)

19 February 2025

Output-only damage diagnosis for plan-symmetric buildings with asymmetric damage using modal flexibility-based deflections

Giacomo Bernagozzi[1,*], Carlos E. Ventura[2], Saeid Allahdadian[2], Yavuz Kaya[3], Luca Landi[1], Pier Paolo Diotallevi[1]

[1] *Department DICAM, University of Bologna, Bologna, Italy*

[2] *Department of Civil Engineering, The University of British Columbia, Vancouver, Canada*

[3] *British Columbia Ministry of Transportation and Infrastructure*

ABSTRACT

Effective methods for vibration-based damage diagnosis in building structures are based on the estimation of structural deflections from identified modal flexibility (MF) matrices. However, most of the existing methods and previous studies that use MF-based deflections were developed by considering the case of buildings that can be modeled as planar structures (e.g. plan-symmetric buildings) both in the baseline and possibly damaged states. In an attempt to fill this research gap, a deflection-based method for output-only damage diagnosis in building structures tested under ambient vibrations is proposed in this paper. The method is applicable for simple rectangular plan-symmetric "box type" 3D building structures which may experience asymmetric damage, and it can be used for detecting, localizing and quantifying the damage. One of the main differences between the proposed and the existing methods is related to the inspection loads adopted to estimate the MF-based deflections. The inspection loads of the proposed method are more complex than the uniform translational loads adopted in the existing methods. Such proposed loads in fact can be assembled only after having estimated the position of the center of stiffness for each story of the structure. According to the proposed approach, the locations of the centers of stiffness are extracted from the experimentally-derived modal flexibility matrices, before performing the damage diagnosis process. The effectiveness and validity of the proposed method was demonstrated both through numerical analyses and by executing experimental ambient vibration tests on a frame building. The results of

[*] Corresponding author: Giacomo Bernagozzi; email: giacomo.bernagozzi2@unibo.it

the proposed method were also compared with the existing approach which was developed for planar structures. This comparison (made both through numerical and experimental analyses) demonstrated that only the proposed approach can be used to perform a correct damage diagnosis process in plan-symmetric buildings which may experience asymmetric damage, especially when considering the damage quantification problem.

Keywords: structural health monitoring, damage detection, output-only modal identification, modal flexibility-based deflection, building.

1 Introduction

Deciding whether a structure is damaged or not starting from acquired vibration data is one of the main tasks that one expects to accomplish when applying Structural Health Monitoring (SHM) strategies and techniques [1-3]. Applications of such techniques can be found, for example, in civil, mechanical, and aerospace engineering structures. The monitoring process is in general performed during the normal operating conditions of the structures, and, especially for civil engineering structures, the ambient vibration responses are usually measured. Vibration-based techniques for damage detection work on the premise that the dynamic and mechanical properties are generally modified due to the occurrence of damage, and thus such techniques aim at identifying changes in the vibration responses and behavior of the structure that can be associated to a damaged state. Of course, not all the changes might be due to damage, since for example, as discussed in [2-4], the dynamic properties (such as the modal parameters) of structures may also be affected by changes in the environmental and operational conditions. The considered techniques can be used not only to detect the existence of damage in the structure, but they can also be used for localizing and quantifying the damage. This type of analysis, which includes the damage detection, localization and quantification, is usually referred to as damage diagnosis [3].

Effective methods for vibration-based damage detection (VBDD) use structural deflections computed from modal flexibility. Such methods were applied to various types of structures, such as

bridges [5-8] and buildings [9-14]. In all these methods the major operation to be performed is to estimate modal flexibility matrices of the structure. Subsequently, special loads (which vary depending on the considered type of structure and which are denoted as "inspection loads") are applied to estimate the deflections. Such methods can thus be considered as a subclass of the modal flexibility-based methods [5-12,14-16], which in turn are a subclass of the modal parameter-based methods [1,3] for VBDD. Referring to the effectiveness and robustness of the considered methods, in [17] it was shown that the coefficients of the modal flexibility matrices are more sensitive to damage than the modal parameters individually (i.e. natural frequencies and components of the mode shapes). In addition, in [9,10,18] it was shown that the components of modal flexibility-based deflections due to uniform loads are less sensitive to experimental errors and modal truncation effects than the components of the modal flexibility matrices.

Referring specifically to building structures, a recently developed method for vibration-based damage diagnosis based on the use of modal flexibility-based deflections has been presented in [9-11]. A special type of inspection loads, denoted as positive shear inspection loads (PSIL) [9], are applied to evaluate the deflections, and then, according to the method (hereinafter referred to as PSIL method, for brevity), the interstory drifts of the deflections are determined and used as damage sensitive features (DSFs). It is important to underline that the PSIL method was formulated for structures that can be modeled as planar structures both in the pristine and damaged states, and its effectiveness was thus verified through output-only vibration tests on building structures with plan-symmetric configurations. These vibration tests were performed using uniaxial white noise excitations in shaking table tests [9,10] or shaker tests [11], and then 2D analyses were performed to estimate the modal flexibility matrices and the deflections of the structures in the direction of the uniaxial excitation.

In practice, the real structures are more complex than planar structures. As observed in [19,20], several real-life building structures are plan-asymmetric (for example, they are characterized by a generic distribution of the stiffness and the mass of the different stories). Alternatively, even if

the structure considered in the damage detection process as the pristine structure is plan-symmetric, the structure can then experience damage in a generic position of any story. The structure in the damaged state can thus be a plan-asymmetric structure, which can not be modeled as a planar structure. It is thus clear that it could be of interest to have a damage detection technique that exploits the same advantages of the existing VBDD methods that use MF-based deflections (like the PSIL method), but that (differently from the PSIL method) can be applied on 3D building structures. Developing VBDD methods to be applied on 3D plan-asymmetric building structures is a problem that has been also addressed in previous recent researches [19-21], by considering methods different from the ones that use MF-based deflections. An approach that use a modal parameter-based story damage index developed for planar building structures (which was presented in [22]) has been recently extended to deal with the case of torsionally coupled buildings, as shown in [21]. In [21] a comparison is also made between the planar and 3D formulations of the method to evaluate the errors obtained in the damage detection process when the torsional coupling effects are ignored. In [19,20] a multi-criteria approach for damage detection in asymmetric buildings has been presented. The damage indices adopted in [19,20] are modified versions of the indices traditionally used in the modal strain energy method [23,24] and in the modal flexibility method [15].

The objective of the paper is to propose a deflection-based method for output-only damage diagnosis in building structures tested under ambient vibrations. The proposed method is applicable for simple rectangular plan-symmetric "box type" 3D building structures which may experience asymmetric damage. This method is an extension of the existing PSIL method developed for planar structures (both in the baseline and possibly damaged states). The proposed method thus extends the PSIL method to the case of more complex building structures (including torsional response). The proposed method is able to localize the damage in the building (by identifying stories and directions of the structure that have been affected by the damage), and to provide an estimate of the damage severity. The present paper can be considered as a continuation of a previous and preliminary work by the authors [13], where a substantially equivalent version of the existing PSIL method has been

applied to plan-symmetric structures with either symmetric or asymmetric damage. This analysis performed in the previous work [13] showed some of the limitations of applying the existing PSIL method on plan-symmetric structures with asymmetric damage, and such limitations are overcome by the approach proposed in this paper.

The article is organized as follows. Section 2 summarizes the main steps of the existing PSIL method (i.e. theoretical background). Section 3 is dedicated to the description of the proposed method for damage diagnosis. Section 4 shows how the proposed method was derived, and also shows how the errors introduced when applying the PSIL method to plan-symmetric structures with asymmetric damage are corrected using the proposed method. Section 5 presents the verification and validation of the proposed method, which were performed, respectively, through numerical analyses and by executing experimental ambient vibration tests on a frame building.

2 Theoretical background: deflection-based damage diagnosis for plan-symmetric buildings with symmetric damage

Damage diagnosis in building structures can be performed using the Positive Shear Inspection Load (PSIL) method [9-11], presented in Figs. 1a, 2a and summarized in this section. This methodology is applicable for structures that can be modeled as planar shear-type buildings both for the baseline (or undamaged) state and in the inspection phase (i.e. for the possibly damaged state) [9], and ambient vibration (AV) tests have to be executed by acquiring horizontal acceleration measurements at all the stories of the building. The acquired data is analyzed using any output-only modal identification technique [25] to extract the modal parameters, and then modal flexibility matrices of the building are estimated. When doing this operation mass-normalized mode shapes are required and can be determined by estimating a-priori the mass matrix of the structure [9] or using the added mass method [26,27]. If one follows the first approach, as done in [9], the modal flexibility matrix $\boldsymbol{F_r}_{n\times n}$ can be obtained as follows

$$\boldsymbol{F_r}_{n\times n} = \boldsymbol{\Psi_r}\,\boldsymbol{\Lambda_r^{-1}}(\boldsymbol{\Psi_r^T}\,\mathbf{M}\,\boldsymbol{\Psi_r})^{-1}\,\boldsymbol{\Psi_r^T} \quad (1)$$

which is an expression valid for a generic MDOF classically-damped structure [16], here applied for a planar shear building. In Eq. (1), n is the total number of the DOFs (equal to the number of the stories for the considered structure), r ($\leq n$) is the number of the included modes, each column of $\boldsymbol{\Psi}_{\boldsymbol{r}\ n\times r}$ is a real arbitrarily-scaled mode shape, $\boldsymbol{M}_{n\times n}$ is the (diagonal) mass matrix, $\boldsymbol{\Lambda}_{\boldsymbol{r}\ r\times r}$ is a diagonal matrix and each term of its diagonal is ω_i^2 (where ω_i is the i-th natural circular frequency and i=1…r).

The deflection of the building is then determined from the modal flexibility matrix

$$\boldsymbol{\chi} = \boldsymbol{F}_{\boldsymbol{r}}\,\boldsymbol{p} \tag{2}$$

where $\boldsymbol{p}_{n\times 1}$ is a positive shear inspection load (PSIL), i.e. a load that generates a positive story shear in all the stories of the structure [9]. Among the different PSIL loads that can be selected, in [9] it is recommended to use a uniform load (UL) $\boldsymbol{p} = \{1 \quad 1 \quad ... \quad 1\}^T$ (Fig. 1a). Starting from the deflection, the interstory drifts - i.e. the damage-sensitive features in the PSIL method - are determined

$$\delta_j = \begin{cases} \chi_j - \chi_{j-1} & for\ j = 2\ldots n \\ \chi_j & for\ j = 1 \end{cases} \tag{3}$$

All the steps described so far are applied both in the baseline and inspection phases, and the modal flexibility matrices are usually estimated using the same number of modes ($r_B = r_I = r$). When the damage detection problem is interpreted as a pattern recognition problem [3], the data sets related to the baseline and inspection phases are usually denoted as training and testing data sets, respectively. In the ideal case of having exact modal parameters and no modal truncation errors [28], the j-th story of the building is considered as damaged if $\Delta\delta_j = \delta_{I,j} - \delta_{B,j} > 0$ [9]. Of course, the DSFs are affected by uncertainties, and thus in the PSIL method a statistical criterion based on the evaluation of the following index z_j is adopted in the damage detection and localization process

$$z_j = \frac{\delta_{I,j} - \bar{\delta}_{B,j}}{s(\delta_{B,j})} \tag{4}$$

where $\delta_{I,j}$ is the interstory drift determined from the testing data set, and $\bar{\delta}_{B,j}$ and $s(\delta_{B,j})$ are the sample mean and the sample standard deviation of the interstory drifts $\delta_{B,j,i}$ estimated from the

training data set (for $i = 1 \ldots q$ where q is the total number of extracted DSFs). Assuming that such interstory drifts $\delta_{B,j,i}$ have a normal distribution, the presence of damage is detected if $z_j > z^{TH}$ at least for one story (detection), and each story for which $z_j > z^{TH}$ is identified as damaged (localization), where z^{TH} is a user-selectable threshold. In [9], for example, $z^{TH} = 2.5$ is considered.

For the stories that have been identified as damaged the damage quantification can be carried out by evaluating the index α (damage severity) [10,11] – i.e. an index in the range from 0 (no damage) to 1 (completely damaged story) that represents the relative portion of the story stiffness lost as a result of the damage occurrence. For the *j*-th story the index α can be estimated as

$$\alpha_j = \frac{\delta_{I,j} - \bar{\delta}_{B,j}}{\delta_{I,j}} \tag{5}$$

3 Proposed damage diagnosis method for plan-symmetric buildings with asymmetric damage using modal flexibility-based deflections

The proposed method is able to deal with simple rectangular "box type" 3D building structures (Fig. 1b), and it extends the existing PSIL method (developed for planar buildings) to the case of such more complex structures. It is assumed that the structures considered in the proposed method can be modeled as shear-type buildings (similarly to the PSIL method) and that each floor of the building has a rigid-body in-plane behavior. Other two assumptions were introduced: 1) due to the characteristics of the considered structures (i.e. simple rectangular "box type" 3D buildings), the geometric center (GC) of each floor of the structure can be reasonably assumed as the center of mass (CM); 2) it is assumed that the baseline structure has a plan-symmetric distribution of the story stiffness at all the stories. Then, the structure can experience damage in a generic position of any story, and thus the structure related to the inspection stage has a generic (either plan-symmetric or plan-asymmetric) distribution of the story stiffness at the different stories. These last two above-mentioned assumptions were introduced to simplify the analyzed problem and to start developing an approach that deals with 3D structures, instead of planar ones. It is expected that the proposed procedure can be eventually modified and extended to deal with structures that are more complex

than rectangular “box type” buildings and that are characterized by generic positions of the centers of mass and stiffness (both in the baseline and inspection phases). However, this is part of a larger problem that will be the object of future developments of the research.

The proposed method for damage diagnosis can be applied starting from the responses of the structure under ambient vibrations, and, similarly to the PSIL method, acceleration measurements have to be available at all the stories of the structure (both in the baseline and inspection phases). The proposed procedure is implemented as follows:

1. Extraction of the modal parameters from output-only vibration data;
2. Estimation of the modal flexibility matrices of the building structures;
3. Estimation of the positions of the centers of stiffness;
4. Computation of the proposed inspection loads;
5. Estimation of the modal flexibility-based deflections of the building structures;
6. Estimation of the modal flexibility-based interstory movements;
7. Detection and localization of the damage;
8. Quantification of the damage.

In the proposed approach it is important to capture the dynamic modal behaviour of the 3D building structure (in the main directions x, y, and around the vertical axis), and this can be obtained when considering at least three measurements of horizontal accelerations (in different locations and directions) at each story of the structure. An example of a sensor layout to be used in the AV test is reported in Fig. 1b. If one performs the AV test by acquiring only one data set with fixed sensors, the number of the sensors should be equal to $3n$, where n is the total number of the stories. If one acquires multiple data sets by adopting both reference and roving sensors (i.e. fixed and moving sensors) [25], then a lower number of sensors can be used in the test.

The steps of the proposed procedure are shown in the flow chart of Fig. 2b and are described in the following:

1. Starting from the vibration data, the modal parameters in terms of natural frequencies and mode shapes are identified using any output-only modal identification technique [25]. Then, under the assumption of having floors of the structure with a rigid-body in-plane behavior, the mode shapes identified at sensor locations are transformed and evaluated in the geometric center of the structure. The components of a generic *i*-th mode shape can be collected in a $3n \times 1$ vector $\boldsymbol{\psi_i} = \{ \boldsymbol{\psi}_{i,n}^T \quad \dots \quad \boldsymbol{\psi}_{i,j}^T \quad \dots \quad \boldsymbol{\psi}_{i,1}^T \}^T$, where $\boldsymbol{\psi_{i,j}} = \{ \psi_{i,j,x} \quad \psi_{i,j,y} \quad \psi_{i,j,\theta} \}^T$ for j=1…n and where $\psi_{i,j,x}$, $\psi_{i,j,y}$, $\psi_{i,j,\theta}$ are, respectively, the component in x direction, the component in y direction and the rotational component. For the case in which a multi-setup operational modal analysis (OMA) test is performed using a limited number of sensors, existing techniques for mode shape merging can be adopted [25].

2. The modal flexibility matrices of the 3D building structure are determined, by adopting a modal scaling technique. For example, when an a-priori estimate of the system mass matrix is used (as done in the PSIL method), the modal flexibility matrix is determined as follows

$$\boldsymbol{F_r}_{3n \times 3n} = \boldsymbol{\Psi_r} \boldsymbol{\Lambda_r^{-1}} (\boldsymbol{\Psi_r^T} \mathbf{M} \boldsymbol{\Psi_r})^{-1} \boldsymbol{\Psi_r^T} \tag{6}$$

Eq. (6) is similar to Eq. (1), but now in Eq. (6) $\boldsymbol{F_r}$ and $\mathbf{M}$ are $3n \times 3n$ matrices and $\boldsymbol{\Psi_r}$ is a $3n \times r$ matrix. The steps no. 1 and 2 are repeated both for the undamaged and the possibly damaged structures.

3. At this stage, the positions of the centers of stiffness (CK) for each story of the structure (i.e. the values of the eccentricities $e_{y,j}$ and $e_{x,j}$ shown in Fig. 1b) have to be determined, and such information is included in the modal flexibility matrices estimated at step no. 2. To this purpose, a load $\boldsymbol{p_\theta}$ which consists only of unitary torques applied at all the floor levels is considered – i.e. $\boldsymbol{p_\theta} = \{ \boldsymbol{p}_{\theta,n}^T \quad \dots \quad \boldsymbol{p}_{\theta,j}^T \quad \dots \quad \boldsymbol{p}_{\theta,1}^T \}^T$ where $\boldsymbol{p_{\theta,j}} = \{ 0 \quad 0 \quad 1 \}^T$ for j=1…n. Then, the modal flexibility-based deflection of the 3D structure due to the load $\boldsymbol{p_\theta}$ is determined

$$\boldsymbol{\chi_\theta} = \boldsymbol{F_r} \boldsymbol{p_\theta} \tag{7}$$

where the subscript θ is explicitly introduced to indicate that the deflection is evaluated for such specific load $\boldsymbol{p_\theta}$. The vector of the deflection $\boldsymbol{\chi_\theta} = \{\, \boldsymbol{\chi}_{\boldsymbol{\theta,n}}^T \quad \dots \quad \boldsymbol{\chi}_{\boldsymbol{\theta,j}}^T \quad \dots \quad \boldsymbol{\chi}_{\boldsymbol{\theta,1}}^T \,\}^T$ is composed by sub-vectors $\boldsymbol{\chi_{\theta,j}} = \{\, u_{\theta,j} \quad v_{\theta,j} \quad \theta_{\theta,j} \,\}^T$, where $u_{\theta,j}$, $v_{\theta,j}$, and $\theta_{\theta,j}$ are, respectively, the component in the *x* direction, the component in the *y* direction and the rotation around the vertical axis of the MF-based deflection evaluated in the geometric center of the structure. Such components are indicated with different symbols for clarity. Starting from the MF-based deflection in Eq. (7), the vector of the interstory movements (i.e. interstory drifts and interstory rotations) $\boldsymbol{\delta_\theta} = \left\{ \boldsymbol{\delta}_{\boldsymbol{\theta,n}}^T \quad \dots \quad \boldsymbol{\delta}_{\boldsymbol{\theta,j}}^T \quad \dots \quad \boldsymbol{\delta}_{\boldsymbol{\theta,1}}^T \right\}^T$ is determined, where each sub-vector $\boldsymbol{\delta_{\theta,j}}$ is as follows

$$\boldsymbol{\delta_{\theta,j}} = \begin{cases} \boldsymbol{\chi_{\theta,j}} - \boldsymbol{\chi_{\theta,j-1}} & for\ j = 2 \dots n \\ \boldsymbol{\chi_{\theta,j}} & for\ j = 1 \end{cases} \tag{8}$$

The components of the vector $\boldsymbol{\delta_{\theta,j}}$ are indicated as follows $\boldsymbol{\delta_{\theta,j}} = \{\, \Delta u_{\theta,j} \quad \Delta v_{\theta,j} \quad \Delta\theta_{\theta,j} \,\}^T$. Finally, the values of the eccentricities can be estimated to identify the position of the center of stiffness of the generic *j*-th story of the structure. If $\left|\Delta u_{\theta,j}\right| \leq \Delta u_\theta^{TH}$, then $e_{y,j} = 0$. If $\left|\Delta u_{\theta,j}\right| > \Delta u_\theta^{TH}$, then

$$e_{y,j} = \frac{\Delta u_{\theta,j}}{\Delta\theta_{\theta,j}} \tag{9}$$

If $\left|\Delta v_{\theta,j}\right| \leq \Delta v_\theta^{TH}$, then $e_{x,j} = 0$. If $\left|\Delta v_{\theta,j}\right| > \Delta v_\theta^{TH}$, then

$$e_{x,j} = -\frac{\Delta v_{\theta,j}}{\Delta\theta_{\theta,j}} \tag{10}$$

where Δu_θ^{TH} and Δv_θ^{TH} are threshold values determined according to the procedure outlined in Section 3.1. Of course, $\left|e_{y,j}\right|$ should be $\leq \frac{L_y}{2}$ and $\left|e_{x,j}\right|$ should be $\leq \frac{L_x}{2}$, where L_y and L_x are the dimensions of the plan of the structure in the *y* and *x* directions, respectively (Fig. 1b). For the possibly damaged structure (i.e. inspection phase), Eqs. (9,10) are used to determine the values of the eccentricities $e_{y,I,j}$ and $e_{x,I,j}$ for each story *j*=1 … *n*. On the contrary, as already mentioned, the baseline structure is assumed to be plan-symmetric and thus the values of the eccentricities are set to zero ($e_{y,B,j} = 0$ and $e_{x,B,j} = 0$). As shown later in Section 3.1, the data related to the baseline structure are used to

determine the thresholds Δu_θ^{TH} and Δv_θ^{TH}, which, in turn, are essential to identify the eventual presence of a plan-asymmetric condition in the inspection stage.

4. Similarly to the PSIL method, in the proposed approach positive shear inspection loads have to be applied to the identified MF-based models of the structure in order to perform the damage diagnosis process. However, differently from the existing method developed for planar structures, in the proposed approach two different and separate analyses have to be performed, one for each of the two prevalent directions of the "box type" building structure (i.e. the *x* and *y* directions). In addition, the inspection loads of the proposed approach are different from the uniform loads (UL) considered in the existing method (shown in Section 2). The inspection loads adopted in the 3D case include not only translational uniform components but also torsional components (i.e. torques applied at the different floor levels), and are thus indicated as UL+T loads. The inspection load (ULx+T) to be applied for the analysis in *x* direction is $\boldsymbol{p_x} = \{\, \boldsymbol{p_{x,n}^T} \quad \dots \quad \boldsymbol{p_{x,j}^T} \quad \dots \quad \boldsymbol{p_{x,1}^T} \,\}^T$ where $\boldsymbol{p_{x,j}} = \{\, 1 \quad 0 \quad t_{x,j} \,\}^T$ for j=1…n and the torque $t_{x,j}$ is defined as

$$t_{x,j} = \begin{cases} -1\, e_{y,j} & for\ j = n \\ (n-j)\, e_{y,j+1} - (n-j+1)\, e_{y,j} & for\ j = 1 \dots (n-1) \end{cases} \tag{11}$$

The inspection load (ULy+T) to be used for the analysis in *y* direction is $\boldsymbol{p_y} = \{\, \boldsymbol{p_{y,n}^T} \quad \dots \quad \boldsymbol{p_{y,j}^T} \quad \dots \quad \boldsymbol{p_{y,1}^T} \,\}^T$ where $\boldsymbol{p_{y,j}} = \{\, 0 \quad 1 \quad t_{y,j} \,\}^T$ for j=1…n and the torque $t_{y,j}$ is as follows

$$t_{y,j} = \begin{cases} 1\, e_{x,j} & for\ j = n \\ -(n-j)\, e_{x,j+1} + (n-j+1)\, e_{x,j} & for\ j = 1 \dots (n-1) \end{cases} \tag{12}$$

The values of the eccentricities $e_{y,j}$ and $e_{x,j}$ (j=1…n) used in Eqs. (11,12) are obtained from step no. 3. In Eqs. (11,12) each coefficient that multiplies the eccentricities is the story shear that is induced in each story of the building structure by the translational uniform loads in *x* and *y* directions, respectively (as demonstrated in Section 4.1).

5. The inspection loads defined at step no. 4 are adopted to evaluate the modal flexibility-based deflections of the building structure. For the analyses in *x* and *y* directions, respectively, the deflections are as follows

$$\boldsymbol{\chi_x} = \boldsymbol{F_r}\,\boldsymbol{p_x} \quad ; \quad \boldsymbol{\chi_y} = \boldsymbol{F_r}\,\boldsymbol{p_y} \tag{13}$$

Such deflections have components defined with respect to the geometric center of the structure, similarly to the deflection evaluated using Eq. (7). In Eq. (13) the subscript *x* (*y*) indicates that the deflection is evaluated for the load $\boldsymbol{p_x}$ ($\boldsymbol{p_y}$).

6. Using the same criterion defined at step no. 3 and specifically in Eq. (8), the vectors of the interstory movements are evaluated from the MF-based deflections reported in Eq. (13). Such vectors are indicated as $\boldsymbol{\delta_x}$ and $\boldsymbol{\delta_y}$ for the analyses in *x* and *y* directions, respectively. The steps 4-6 have to be repeated both for the undamaged and the possibly damaged structures. Then, the criteria for damage detection, localization and quantification of the existing PSIL method developed for planar structures are modified and adapted to the case of the "box type" 3D structures, where according to the proposed approach the analyses are performed in the two main directions *x* and *y*.

7. Damage is present at the *j*-th story in the *x* (*y*) direction of the building structure if $\Delta u_{I,x,j} - \Delta u_{B,x,j} > 0$ ($\Delta v_{I,x,j} - \Delta v_{B,x,j} > 0$), where $\Delta u_{I,x,j}$, $\Delta u_{B,x,j}$ ($\Delta v_{I,x,j}$, $\Delta v_{B,x,j}$) are the interstory drifts in x (y) direction of the MF-based deflection $\boldsymbol{\chi_x}$ ($\boldsymbol{\chi_y}$) evaluated for the load $\boldsymbol{p_x}$ ($\boldsymbol{p_y}$) in the inspection and baseline phases, respectively. The statistical approach for outlier detection [3,29] based on the z-index (Eq. 4) is adapted in the proposed approach for performing the analyses in the two main directions *x* and *y*

$$z_{x,j} = \frac{\Delta u_{I,x,j} - \Delta \bar{u}_{B,x,j}}{s(\Delta u_{B,x,j})} \quad ; \quad z_{y,j} = \frac{\Delta v_{I,y,j} - \Delta \bar{v}_{B,y,j}}{s(\Delta v_{B,y,j})} \tag{14}$$

where, as already mentioned in Section 2, the operators $\bar{\cdot}$ and $s(\cdot)$ indicate the sample mean and the sample standard deviation, respectively, and are applied on the interstory drifts $\Delta u_{B,x,j,h}$ ($\Delta v_{B,y,j,h}$) evaluated for the baseline state for h=1 … q. Damage is detected, and its location is identified at the *j*-th story in *x* (*y*) direction if $z_{x,j} > z^{TH}$ ($z_{y,j} > z^{TH}$). As already mentioned in Section 2, the user

can select the threshold z^{TH} (to control the trade off between false negatives and false positives). In the analyses of this paper, the threshold was set as $z^{TH} = 3$ to reduce the probability of obtaining false positives from the z-index test (as also done in [13,14]). In other words, assuming that the baseline DSFs have a normal distribution, the DSF related to the inspection state is considered as an outlier if it is more than 3 standard deviations from the mean value of the baseline. In presence of changing environmental conditions, the potential approach, discussed but not applied in the work that proposed the PSIL method [9], could also be adopted for the z indices of Eq. (14) – i.e. modifying the index z_j to account for temperature effects, as proposed in [6] for bridge structures. Dealing with temperature variations is, however, not part of the present work, and dedicated experimental researches could be carried out in the future to apply in these conditions both the existing PSIL method, valid for planar structures, and the proposed extended method.

8. If a story of the 3D building structure is classified as damaged in the *x* or *y* direction using the criteria of step no. 7, the damage severity at the *j*-th story can be estimated in the *x* or *y* direction, respectively, as follows

$$\alpha_{x,j} = \frac{\Delta u_{I,x,j} - \Delta \bar{u}_{B,x,j}}{\Delta u_{I,x,j}} \quad ; \quad \alpha_{y,j} = \frac{\Delta v_{I,y,j} - \Delta \bar{v}_{B,y,j}}{\Delta v_{I,y,j}} \tag{15}$$

where, similarly to Eq. (5), $\alpha_{x,j}$ and $\alpha_{y,j}$ are relative indices in the range from 0 to 1. Eq. (15) provides the average value of the damage severity, while the dispersion on the damage severity can be estimated starting from the values of damage severity evaluated for each *h*-th portion of the training data set ($h = 1 \dots q$) – i.e. using the following modified version of Eq. (15) where the sample mean of the interstory drifts related to the baseline structure is replaced by the drift estimated for each *h*-th portion of the training data set

$$\alpha_{x,j,h} = \frac{\Delta u_{I,x,j} - \Delta u_{B,x,j,h}}{\Delta u_{I,x,j}} \quad ; \quad \alpha_{y,j,h} = \frac{\Delta v_{I,y,j} - \Delta v_{B,y,j,h}}{\Delta v_{I,y,j}} \tag{16}$$

Then, the dispersion can be estimated, for example, as the sample standard deviation of the quantities obtained using Eq. (16). Of course, better estimates of the damage severity (and its dispersion) could be obtained by measuring wider testing data sets and by estimating more than one value of the

interstory drift in each direction for the structure in the inspection phase. However, in the present paper it is assumed to deal with the minimum amount of training/testing data sets required to detect and localize the damage using the adopted criterion for outlier analysis (step no. 7), and considering wider testing data sets could be done in future developments of the research.

The main differences between the approach proposed for "box type" 3D building structures and the existing PSIL method valid for planar structures can be summarized as follows:

a) An experimentally identified $3n$-DOF model of the structure is considered in the proposed approach, instead of the n-DOF model considered in the PSIL method.

b) Two separate analyses in the main directions of the "box type" structure are considered in the proposed approach, instead of one analysis performed for the planar structure in the PSIL method.

c) Differently from the PSIL method, the inspection loads considered in the proposed approach include not only translational components, but also torsional components. Such torques are specifically introduced to avoid relative rotations between the floor levels in the MF-based deflections used in the damage diagnosis process. As shown in Eqs. (11,12), the torques depend on the values of the eccentricities $e_{y,j}$ and $e_{x,j}$, and thus the step related to the estimation of the position of the centers of stiffness (step no. 3) is a fundamental step, not present in the existing PSIL method, that is added in the proposed approach.

Of course, when the "box-type" structure considered in the inspection phase has a plan-symmetric distribution of the story stiffness at all the stories, the proposed method provides the same results that can be obtained by performing a planar (2D) analysis on the structure using the existing PSIL method.

3.1 Determination of the thresholds used to identify the plan-asymmetric stories

In step no. 3 of the proposed procedure (Section 3) a statistical test is introduced to identify the stories of the structure related to the inspection phase that have a plan-asymmetric distribution of the story stiffness – i.e. only when the interstory drifts of the MF-based deflection $\boldsymbol{\chi_\theta}$ exceed the threshold values Δu_θ^{TH} and Δv_θ^{TH}, the values of the eccentricities $e_{y,j}$ and $e_{x,j}$ are determined according to Eqs.

(9,10). In the proposed method, this statistical approach was introduced to deal with the fact that all the quantities identified from experimental noisy vibration data (for example in such case the MF-based interstory drifts due to the load $\boldsymbol{p_\theta}$) are affected by uncertainties. In presence of such uncertainties, in fact, evaluating the eccentricities using Eqs. (9,10) without performing the proposed statistical test might not be a robust and stable approach. For example, for plan-symmetric stories some spurious eccentricities (which are not real, but only due to the presence of noise) might be obtained from the calculations, and the statistical approach was introduced in the proposed method to avoid or limit these effects as much as possible.

According to the proposed approach, the threshold values Δu_θ^{TH} and Δv_θ^{TH} are obtained using an empirical procedure that uses the data related to the baseline structure, which, as already mentioned, is assumed to have a plan-symmetric distribution of the story stiffness at all the stories. The thresholds Δu_θ^{TH} and Δv_θ^{TH} are obtained through the following steps. The modal flexibility-based deflections due to the load $\boldsymbol{p_\theta}$ are evaluated for the baseline structure starting from modal flexibility matrices assembled from the training data set (i.e. for each *h*-th portion of the training data set for *h* = 1… *q*)

$$\boldsymbol{\chi_{\theta,h}} = \boldsymbol{F_{r,h}}\, \boldsymbol{p_\theta} \tag{17}$$

Then, using the same criterion defined at step no. 3 and specifically in Eq. (8), the vectors of the interstory movements $\boldsymbol{\delta_{\theta,h}}$ are determined from the MF-based deflections $\boldsymbol{\chi_{\theta,h}}$ (Eq. 17). The components of such vectors are indicated as $\boldsymbol{\delta_{\theta,h}} = \left\{ \boldsymbol{\delta}_{\boldsymbol{\theta,n,h}}^T \quad \dots \quad \boldsymbol{\delta}_{\boldsymbol{\theta,j,h}}^T \quad \dots \quad \boldsymbol{\delta}_{\boldsymbol{\theta,1,h}}^T \right\}^T$ where $\boldsymbol{\delta_{\theta,j,h}} = \{ \Delta u_{\theta,j,h} \quad \Delta v_{\theta,j,h} \quad \Delta\theta_{\theta,j,h} \}^T$. Finally, the threshold value Δu_θ^{TH} is determined as follows

$$\Delta u_\theta^{TH} = \max_{j=1\dots n} \left\{ \max_{b=b_1;\, b=b_2} \left| \mathrm{b^{th}} \operatorname*{percentile}_{h=1\dots q} \left(\Delta u_{\theta,j,h} \right) \right| \right\} \tag{18}$$

while the threshold Δv_θ^{TH} is obtained by performing the same operations shown in Eq. (18) but starting from the drifts $\Delta v_{\theta,j,h}$ (instead of the drifts $\Delta u_{\theta,j,h}$, reported in Eq. 18). In Eq. (18) the terms b_1 and b_2 express the percentages that are used for the evaluation of the percentiles from the considered data

sets of drifts, and are user-selectable constants. According to the typical values assumed in the literature, as shown for example in [3,30], b_1 ranges from 0 to 5 and b_2 ranges from 95 to 100. In the present study these parameters were set as b_1=0.1 and b_2=99.9, i.e. assuming a normal distribution each of these two percentages is related to a value of the percentile that is 3 standard deviations away from the mean.

4 Derivation of the proposed method

4.1 Derivation of the proposed inspection loads

This section presents the strategy that was followed to derive the proposed approach and the related inspection loads (i.e. UL+T loads). According to the existing PSIL method (Section 2) a 2D analysis is performed on a planar structure – i.e. the inspection loads and the MF-based deflections are characterized by components only in one direction. On the contrary, if one applies the same types of loads (i.e. only translational loads in one direction) on a "box type" 3D building structure characterized by generic (e.g. plan-asymmetric) distributions of the story stiffness, it is clear that the MF-based deflections might be coupled in the three directions (i.e. *x*-, *y*-, and θ directions). The strategy adopted to develop the proposed approach was to find inspection loads that are able to decouple the MF-based deflections – i.e. to provide MF-based deflections of the "box type" 3D structure that are mainly characterized by components in one of the two horizontal directions (i.e. *x* or *y* direction). The analytical formulation and passages adopted to derive the proposed inspection loads are presented in the following.

Let us consider the analytical model of a shear-type "box-type" 3D building structure (i.e. a structure similar to the one considered in Section 3), expressed by its flexibility matrix

$$\boldsymbol{F}_{3n\times 3n} = \begin{bmatrix} \boldsymbol{F_n}+\cdots+\boldsymbol{F_j}+\cdots+\boldsymbol{F_1} & \cdots & \boldsymbol{F_j}+\cdots+\boldsymbol{F_1} & \vdots & \boldsymbol{F_1} \\ \cdots & \ddots & \vdots & \vdots & \boldsymbol{F_1} \\ \boldsymbol{F_j}+\cdots+\boldsymbol{F_1} & \cdots & \boldsymbol{F_j}+\cdots+\boldsymbol{F_1} & \vdots & \boldsymbol{F_1} \\ \cdots & \cdots & \cdots & \ddots & \boldsymbol{F_1} \\ \boldsymbol{F_1} & \boldsymbol{F_1} & \boldsymbol{F_1} & \boldsymbol{F_1} & \boldsymbol{F_1} \end{bmatrix} \tag{19}$$

where each submatrix $\boldsymbol{F_j}$ (j=1…n) can be expressed as

$$\boldsymbol{F_j} = \begin{bmatrix} f_{x,j} + f_{\theta,j} e_{y,j}^2 & -f_{\theta,j} e_{x,j} e_{y,j} & f_{\theta,j} e_{y,j} \\ -f_{\theta,j} e_{x,j} e_{y,j} & f_{y,j} + f_{\theta,j} e_{x,j}^2 & -f_{\theta,j} e_{x,j} \\ f_{\theta,j} e_{y,j} & -f_{\theta,j} e_{x,j} & f_{\theta,j} \end{bmatrix} \tag{20}$$

where $f_{x,j}$, $f_{y,j}$, and $f_{\theta,j}$ are, respectively, the uncoupled flexibility at the j-th story of the structure in x-, y-, and θ directions. The MF-based deflection of the building structure due to a generic load $\boldsymbol{p}$ is as follows

$$\boldsymbol{\chi} = \boldsymbol{F}\,\boldsymbol{p} \tag{21}$$

where, according to the notation used in Section 3, $\boldsymbol{p} = \{\, \boldsymbol{p_n^T} \quad \dots \quad \boldsymbol{p_j^T} \quad \dots \quad \boldsymbol{p_1^T} \,\}^T$ and $\boldsymbol{\chi} = \{\, \boldsymbol{\chi_n^T} \quad \dots \quad \boldsymbol{\chi_j^T} \quad \dots \quad \boldsymbol{\chi_1^T} \,\}^T$. In particular, the components of the deflection at the j-th floor level can be expressed in compact form as

$$\boldsymbol{\chi_j} = \sum_{i=1}^{j} (\boldsymbol{F_i} \sum_{h=i}^{n} \boldsymbol{p_h}) \tag{22}$$

Now let us consider the scenario that one can analyze using the existing PSIL method [9-11]: a) the structure has a plan-symmetric distribution of the story stiffness (or flexibility) at each story, i.e. $e_{x,j} = e_{y,j} = 0$ for each j=1 ... n; b) a generic Positive Shear Inspection Load with components only in the x direction (PSILx) is considered (the components in y direction and the rotational components are zero)

$$\boldsymbol{p_j} = \begin{Bmatrix} p_{j,x} \\ 0 \\ 0 \end{Bmatrix} \tag{23}$$

First of all, it is important to underline that a load whose components $p_{j,x}$ assume generic positive values is here considered (instead of components with unitary values). This is because, as already mentioned in Section 2, the PSIL method is theoretically applicable by considering any of such generic loads, while loads with unitary values are the preferable option to be selected in the calculations. The analytical formulation presented in Section 4 deals with translational loads that are generic positive shear inspection loads, and this formulation is thus also valid for the more specific case of the uniform loads with unitary values.

The MF-based deflection of the considered plan-symmetric structure due to the load shown in Eq. (23) is as follows

$$\boldsymbol{\chi_j^S} = \sum_{i=1}^{j}\left(\boldsymbol{F_i}\sum_{h=i}^{n}\begin{Bmatrix} p_{h,x} \\ 0 \\ 0 \end{Bmatrix}\right) = \sum_{i=1}^{j}\left(\boldsymbol{F_i}\begin{Bmatrix} V_{i,x} \\ 0 \\ 0 \end{Bmatrix}\right) = \sum_{i=1}^{j}\left(V_{i,x}\begin{Bmatrix} f_{x,i} \\ 0 \\ 0 \end{Bmatrix}\right) \tag{24}$$

where $V_{i,x}$ is the story shear induced at the *i*-th story by the loads applied in *x* direction and the superscript *S* indicates that the deflection is evaluated for a plan-symmetric structure.

Now we want to find the load that provides the same deflection of Eq. (24) when applied to an equivalent plan-asymmetric structure - i.e. a structure characterized by values of the uncoupled story stiffness (or flexibility) at each story (in *x*-, *y*-, and θ directions) that are equal to the ones of the plan-symmetric structure, but that is characterized by non-zero values of the eccentricities at the different stories. To achieve this goal, the stiffness matrix of the shear-type "box-type" 3D building structure is considered – i.e.

$$\boldsymbol{K}_{3n\times 3n} = \begin{bmatrix} \boldsymbol{K_n} & -\boldsymbol{K_n} & 0 & \cdots & \cdots & \cdots & \cdots & 0 \\ -\boldsymbol{K_n} & \boldsymbol{K_n}+\boldsymbol{K_{n-1}} & -\boldsymbol{K_{n-1}} & 0 & & & & \vdots \\ 0 & \ddots & \ddots & \ddots & 0 & & & \vdots \\ \vdots & 0 & -\boldsymbol{K_{j+1}} & \boldsymbol{K_{j+1}}+\boldsymbol{K_j} & -\boldsymbol{K_j} & 0 & & \vdots \\ \vdots & & 0 & -\boldsymbol{K_j} & \boldsymbol{K_j}+\boldsymbol{K_{j-1}} & -\boldsymbol{K_{j-1}} & 0 & \vdots \\ \vdots & & & 0 & \ddots & \ddots & \ddots & 0 \\ \vdots & & & & 0 & -\boldsymbol{K_3} & \boldsymbol{K_3}+\boldsymbol{K_2} & -\boldsymbol{K_2} \\ 0 & \cdots & \cdots & \cdots & \cdots & 0 & -\boldsymbol{K_2} & \boldsymbol{K_2}+\boldsymbol{K_1} \end{bmatrix} \tag{25}$$

where each submatrix $\boldsymbol{K_j}$ (*j*=1…*n*) can be expressed as

$$\boldsymbol{K_j} = \begin{bmatrix} k_{x,j} & 0 & -k_{x,j}e_{y,j} \\ 0 & k_{y,j} & k_{y,j}\,e_{x,j} \\ -k_{x,j}e_{y,j} & k_{y,j}\,e_{x,j} & k_{\theta,j}+k_{x,j}e_{y,j}^2+k_{y,j}\,e_{x,j}^2 \end{bmatrix} \tag{26}$$

where $k_{x,j}$, $k_{y,j}$, and $k_{\theta,j}$ are, respectively, the uncoupled stiffness at the *j*-th story of the structure in *x*-, *y*-, and θ directions, as shown in [21]. Then, the following system of equations is considered

$$\boldsymbol{K}\,\boldsymbol{\chi^S} = \boldsymbol{p} \tag{27}$$

where one generic row of the system (i.e. a row formed by submatrices $\boldsymbol{K_j}$ and column subvectors $\boldsymbol{\chi_j^S}$ and $\boldsymbol{p_j}$) can be expressed as follows

$$-\boldsymbol{K_{j+1}\chi_{j+1}^{S}} + \left(\boldsymbol{K_{j+1}} + \boldsymbol{K_j}\right)\boldsymbol{\chi_j^S} - \boldsymbol{K_j\chi_{j-1}^{S}} = \boldsymbol{p_j} \tag{28}$$

By substituting Eqs. (24,26) in the expression on the left-hand side of Eq. (28), the components of the load $\boldsymbol{p_j}$ can be obtained – i.e.

$$\boldsymbol{p_j} = \begin{Bmatrix} p_{j,x} \\ 0 \\ V_{j+1,x}\, e_{y,j+1} - V_{j,x}\, e_{y,j} \end{Bmatrix} \tag{29}$$

Eq. (29) shows the components related to the *j*-th floor level of a Positive Shear Inspection Load applied in *x* direction, which also includes torques (PSILx+T). This load has the following special property. Even if the different stories of the structure are characterized by generic (e.g. plan-asymmetric) distributions of the story stiffness, the MF-based deflection of the structure due to the load PSILx+T has non-zero components only in the *x* direction, while the *y* and rotational components are theoretically zero. Of course, this is true in an ideal unnoisy case. In practice (when the MF-based deflections are estimated from noisy data), the components in *x* direction will be dominating, while the other components will be close to zero.

If the translational loads in x direction of Eq. (29) are set to be equal to uniform loads with unitary values for all floor levels (as suggested in the existing PSIL method valid for planar structures [9]), then the expression of the inspection loads of the proposed method (valid for "box type" 3D building structures) is obtained - i.e. the expression of the ULx+T inspection load proposed in step no. 4 of Section 3. When this operation is performed in fact $p_{j,x}$ of Eq. (29) becomes equal to 1, and the torque of Eq. (29), evaluated for a generic *j*-th floor level, becomes equal to the torque of Eq. (11) for the case *j*=1…(*n* -1). Of course, if the passages of this section are repeated by considering a PSILy load in y direction (instead of the PSILx load in *x* direction, Eq. 23), then the expressions of the inspection loads to be applied in *y* direction according to the proposed method can be obtained – i.e. the general form of a PSILy+T load and the expression of the ULy+T load (proposed in Section 3).

4.2 Observations on the procedure used to determine the position of the centers of stiffness

In this section some observations on the procedure proposed to estimate the position of the centers of stiffness for each story of the "box type" 3D building structure are presented. Such observations are supported by an analytical formulation that, as already done in previous Section 4.1, was derived starting from an analytical model of the structure.

Starting from Eq. (22) (i.e. the MF-based deflection due to a generic load), the interstory movements at the *j*-th story of the structure can be expressed as follows

$$\boldsymbol{\delta_j} = \boldsymbol{F_j} \sum_{h=j}^{n} \boldsymbol{p_h} \tag{30}$$

Now let us assume that the load $\boldsymbol{p_h}$ is composed by rotational components only, i.e. torques with generic values applied at the different floor levels. Eq. (30) can thus be reformulated as follows

$$\boldsymbol{\delta_j} = \boldsymbol{F_j} \sum_{h=j}^{n} \begin{Bmatrix} 0 \\ 0 \\ p_{h,\theta} \end{Bmatrix} = \boldsymbol{F_j} \begin{Bmatrix} 0 \\ 0 \\ T_j \end{Bmatrix} = T_j \begin{Bmatrix} f_{\theta,j} e_{y,j} \\ -f_{\theta,j} e_{x,j} \\ f_{\theta,j} \end{Bmatrix} \tag{31}$$

where T_j is the story torque at the *j*-th story, i.e. the sum of the torques applied at the floor levels above the *j*-th story.

It is clear from Eq. (31) that the interstory movements of a MF-based deflection due to generic torques contain information about the values of the eccentricities. Eq. (31) in fact shows that the values of the eccentricities can be determined by evaluating the ratio between the interstory drifts and the interstory rotations, as done in the proposed method (i.e. step no. 3 of Section 3 and, specifically, Eqs. 9,10). However, Eq. (31) also shows an important condition that has to be fulfilled when performing the above-mentioned operation, i.e. the story torque T_j at each story must not be equal to zero (otherwise the interstory drifts of Eq. 31 are zero, even if the eccentricities $e_{x,j}$ and $e_{y,j}$ are non-zero). To circumvent the problem, for example, torques (to be applied at the different floor levels) that generate positive story torques at all the stories can be selected.

The load considered in step no. 3 of the proposed method (i.e. torques with unitary values applied at all the floor levels) has the above-mentioned characteristic. Among all the loads that has this characteristic, torques with unitary values at all levels were selected as the preferable option for

the same reason for which translational loads with unitary values at all the floor levels are preferred as the inspection loads in the existing PSIL method – i.e. when dealing with noisy data, considering loads with unitary values at all floors is a more robust criterion than considering, for example, a load with unitary value applied only at the top floor [9].

4.3 Observations on the application of PSIL+T and PSIL loads to plan-symmetric buildings with asymmetric damage

A fundamental characteristic of the proposed method is that the adopted inspection loads include not only translational forces but also torques, which in turn depend on the values of the eccentricities. This leads to the need of estimating the positions of the centers of stiffness of the structure from the data, which is thus an operation to be performed before executing the damage diagnosis process. This section deals with the problem of understanding which are the effects and/or the errors that are introduced in the damage diagnosis process on a "box type" 3D building (characterized, for example, by plan-asymmetric stories) when the need of including the torques in the inspection loads is ignored. This problem is analyzed, again, by considering the analytical model of the structure introduced in Section 4.1.

Starting from Eq. (30), let us evaluate at first the interstory movements at the j-th story of the structure due to the application of a PSILx+T load in x direction (i.e. an inspection load which includes torques, Eq. 29)

$$\boldsymbol{\delta_j} = \boldsymbol{F_j} \sum_{h=j}^{n} \begin{Bmatrix} p_{h,x} \\ 0 \\ V_{h+1,x}\, e_{y,h+1} - V_{h,x}\, e_{y,h} \end{Bmatrix} = \boldsymbol{F_j} \begin{Bmatrix} V_{j,x} \\ 0 \\ -V_{j,x} e_{y,j} \end{Bmatrix} = V_{j,x} \begin{Bmatrix} f_{x,j} \\ 0 \\ 0 \end{Bmatrix} \tag{32}$$

Then, let us evaluate the interstory movements that are due to the application of a PSILx load in x direction (i.e. an inspection load which does not includes torques, Eq. 23)

$$\boldsymbol{\delta_j^*} = \boldsymbol{F_j} \sum_{h=j}^{n} \begin{Bmatrix} p_{h,x} \\ 0 \\ 0 \end{Bmatrix} = \boldsymbol{F_j} \begin{Bmatrix} V_{j,x} \\ 0 \\ 0 \end{Bmatrix} = V_{j,x} \begin{Bmatrix} f_{x,j} + f_{\theta,j} e_{y,j}^2 \\ -f_{\theta,j} e_{x,j} e_{y,j} \\ f_{\theta,j} e_{y,j} \end{Bmatrix} \tag{33}$$

where the superscript * indicates that such interstory movements are evaluated for a load (i.e. PSILx) that is different from the proposed inspection loads, and that only for comparative purposes is applied on a generic (either plan-asymmetric or plan-symmetric) story.

At this point, the z index for damage detection/localization and the index related to the damage severity are evaluated both for the PSILx and PSILx+T loads, by assuming that the story of the considered analytical model is plan-asymmetric in the inspection phase and plan-symmetric in the baseline state.

Referring to the problem of the damage detection/localization, the ratio of the z index at the *j*-th story calculated when applying the PSILx load to the z index obtained when applying the PSILx+T load can be expressed as follows

$$\frac{z^*_{x,j}}{z_{x,j}} = \frac{\Delta u^*_{I,x,j} - \Delta \bar{u}^*_{B,x,j}}{s(\Delta u^*_{B,x,j})} \quad \frac{s(\Delta u_{B,x,j})}{\Delta u_{I,x,j} - \Delta \bar{u}_{B,x,j}} \tag{34}$$

where the same notation of Eq. (14) has been adopted. In Eq. (34) the standard deviation of the drifts related to the baseline state cancels out, because quantities evaluated for plan-symmetric stories using the PSILx load are of course equal to the same quantities evaluated for the PSILx+T load. The expressions of the interstory drifts in *x* direction obtained in Eqs. (32,33) can thus be substituted in Eq. (34), which can be rearranged as follows

$$\frac{z^*_{x,j}}{z_{x,j}} = \frac{V_{j,x}}{V_{j,x}} \quad \frac{f_{x,I,j} + f_{\theta,I,j}\, e^2_{y,I,j} - f_{x,B,j}}{f_{x,I,j} - f_{x,B,j}} \tag{35}$$

where the story shear $V_{j,x}$ cancels out because such quantity is the same both for the inspection and baseline phases and when considering both the PSILx and the PSILx+T loads. It is worth noting that the operation of evaluating the sample mean on quantities related to the baseline state (present in Eq. 34) is omitted in Eq. (35), and this is because the analytical formulation of this section has been derived starting from an exact analytical model with no uncertainties. Referring to Eq. (35) it can be observed that: a) all the flexibility coefficients in Eq. (35) are positive; b) in presence of damage it is expected that $f_{x,I,j} > f_{x,B,j}$; c) $e^2_{y,I,j} \geq 0$. By considering the above-mentioned conditions, it is

evident that the expression on the right-hand side of Eq. (35) is ≥ 1, and thus the following important conclusion can be deducted

$$z^*_{x,j} \geq z_{x,j} \tag{36}$$

Referring to the problem of the damage quantification, the damage severity at the *j*-th story calculated when applying the PSILx+T load in *x* direction can be expressed as follows

$$\alpha_{x,j} = \frac{\Delta u_{I,x,j} - \Delta \bar{u}_{B,x,j}}{\Delta u_{I,x,j}} = \frac{V_{j,x}}{V_{j,x}} \frac{f_{x,I,j} - f_{x,B,j}}{f_{x,I,j}} \tag{37}$$

where the expression of the interstory drift in *x* direction obtained in Eq. (32) has been introduced. On the contrary, the damage severity at the *j*-th story evaluated by applying the PSILx load in *x* direction is

$$\alpha^*_{x,j} = \frac{\Delta u^*_{I,x,j} - \Delta \bar{u}^*_{B,x,j}}{\Delta u^*_{I,x,j}} = \frac{V_{j,x}}{V_{j,x}} \frac{f_{x,I,j} + f_{\theta,I,j}\, e^2_{y,I,j} - f_{x,B,j}}{f_{x,I,j} + f_{\theta,I,j}\, e^2_{y,I,j}} \tag{38}$$

where the expression of the interstory drift in *x* direction obtained in Eq. (33) has been inserted, by considering that $e_{y,I,j} \neq 0$ in the inspection phase and $e_{y,B,j} = 0$ for the baseline state. Eq. (38) can then be rearranged in order to express the damage severity obtained for the PSILx load as a function of the damage severity obtained for the PSILx+T load, as follows

$$\alpha^*_{x,j} = c\ \alpha_{x,j} \tag{39}$$

where a coefficient *c* with the following expression has been introduced

$$c = \frac{1 + \frac{f_{\theta,I,j}\, e^2_{y,I,j}}{f_{x,I,j} - f_{x,B,j}}}{1 + \frac{f_{\theta,I,j}\, e^2_{y,I,j}}{f_{x,I,j}}} \tag{40}$$

To understand the relationship between the damage severity evaluated for the PSILx and PSILx+T loads, the values assumed by the coefficient *c* can be analyzed. The already mentioned conditions expressed for Eq. (35) are also valid for Eq. (40), i.e.: a) all the flexibility coefficients in Eq. (40) are positive; b) in presence of damage it is expected that $f_{x,I,j} > f_{x,B,j}$; c) $e^2_{y,I,j} \geq 0$. Thus, it is evident that $c \geq 1$, and this leads to the derivation of the following important conclusion

$$\alpha^*_{x,j} \geq \alpha_{x,j} \tag{41}$$

Of course, all the passages of this section could be repeated by considering inspection loads in *y* direction, and thus the inequalities derived for the z index and the damage severity in *x* direction (i.e. Eqs. 36,41) are also valid for the *y* direction.

The analytical formulation presented so far has shown that, when the stories in the inspection phase become plan-asymmetric (e.g. due to the occurrence of damage in a generic position), both the z index and the damage severity evaluated for PSIL loads are higher than the corresponding indices evaluated for PSIL+T loads. This leads to the following observations that demonstrate the actual need of considering PSIL+T loads instead of PSIL loads when performing a complete damage diagnosis process for the considered structures. As shown at point no. 7 of Section 3, the z-index is used to perform a statistical test to detect and localize the damage. It is thus clear that an overestimation of the z-index obtained at damaged stories when considering PSIL (instead of PSIL+T) loads should theoretically not alter the outcome of the statistical test. On the contrary, the values of the damage severity index are directly used to quantify the damage. Thus, applying PSIL (instead of PSIL+T) loads leads to an overestimation of the damage severity index and to misleading results in the damage quantification process.

The above-mentioned observations formulated by considering the general case of positive shear inspection loads (i.e. PSIL and PSIL+T loads) are also valid for the more specific case in which the considered translational loads are uniform loads with unitary values - i.e. when considering uniform loads without torques (UL) or uniform loads with torques (UL+T). To confirm this statement and to show further evidence of the necessity of adopting the proposed UL+T inspection loads (instead of UL loads) to perform a correct damage diagnosis process, in the numerical and experimental analyses of the paper the proposed method was compared with a procedure based on the use of UL loads. This procedure based on UL loads deals with modal flexibility matrices of the whole “box type” 3D building structures (similarly to the proposed method), but provides the same results of the existing PSIL method developed for planar structures. The procedure based on UL loads was also adopted in the previous and preliminary work by the authors [13], and is summarized herein,

by highlighting the differences with respect to the method proposed in this paper. Steps no. 1 and 2 of Section 3 are applied, while step no. 3 (i.e. estimation of the positions of the centers of stiffness) is skipped. Then, in step no. 4 the proposed UL+T loads are substituted by uniform loads that do not include torques. The load to be applied in x direction (ULx) is $\boldsymbol{p}_{\boldsymbol{x}}^{*} = \{ \boldsymbol{p}_{\boldsymbol{x,n}}^{*\,T} \quad ... \quad \boldsymbol{p}_{\boldsymbol{x,j}}^{*\,T} \quad ... \quad \boldsymbol{p}_{\boldsymbol{x,1}}^{*\,T} \}^{T}$, where $\boldsymbol{p}_{\boldsymbol{x,j}}^{*} = \{ 1 \quad 0 \quad 0 \}^{T}$ for j=1…n, while the load in y direction (ULy) is $\boldsymbol{p}_{\boldsymbol{y}}^{*} = \{ \boldsymbol{p}_{\boldsymbol{y,n}}^{*\,T} \quad ... \quad \boldsymbol{p}_{\boldsymbol{y,j}}^{*\,T} \quad ... \quad \boldsymbol{p}_{\boldsymbol{y,1}}^{*\,T} \}^{T}$, where $\boldsymbol{p}_{\boldsymbol{y,j}}^{*} = \{ 0 \quad 1 \quad 0 \}^{T}$ for j=1…n. Finally, steps from 5 to 8 of Section 3 are applied.

5 Verification and validation of the proposed method

The effectiveness of the proposed method for damage diagnosis in plan-symmetric buildings with asymmetric damage was verified through numerical analyses and by executing experimental vibration tests. In both cases a one-third scale four-story two-bay by two-bay steel frame structure was considered. This structure is located at the Earthquake Engineering Research Facility (EERF) of the University of British Columbia (UBC), Vancouver, Canada. It is worth highlighting that this structure is the same structure that was the object of the benchmark studies for SHM conducted by the IASC-ASCE Task Group, which performed both numerical and experimental studies (i.e. phase I [31,32] and phase II [33-35], respectively).

5.1 Numerical verification

A numerical model of the structure located at UBC was considered in phase I (analytical study) of the IASC-ASCE Task Group. For this purpose, a MATLAB-based finite element (FE) analysis code was developed by the mentioned task group, and then such code was made freely available for the SHM research community (the characteristics of the FE code are described in [31]). This FE code was used in the present study to generate the vibration data sets adopted to numerically verify the proposed damage diagnosis method (which are new data sets different from the ones considered in the benchmark study). As detailed in [31], in the code there are is the possibility to select different

modeling criteria, to define the characteristics of the considered structural configurations (e.g., user-defined damaged configurations), and to specify the parameters and settings for obtaining the vibration responses of the structure. Details about the choices made in the present study with reference to the above-mentioned points are presented herein.

The considered 3D building model is a 12 DOF shear-type model (i.e. 3 DOFs per floor level [31]), which is shown in Fig. 3. The cross-sections of the structural members are double-T sections for columns and beams (B100×9 and S75×11, respectively) and L-shape sections for the diagonal wall braces (L25×25×3), as detailed in [31]. According to the orientation of the column cross-sections, the *x* direction (West-East dir.) is the weak direction of the structure, while the *y* direction (South-North dir.) is the strong direction. It is worth noting that the considered orientation of the whole structural model was modified with respect to the one in [31], to be consistent with the orientation of the real structure in the experimental tests. As shown in Fig. 3b, the model has one floor slab in each bay of each floor level, and, referring to the distribution of these slabs, the slightly plan-asymmetric case reported in [31] was considered with some modifications. In the considered model, the masses of the slabs are 400 kg, 600 kg, 600 kg and 800 kg at the 4^{th}, 3^{rd}, 2^{nd} and 1^{st} story, respectively, except for the slabs located in the south-east bay whose masses are 550 kg, 825 kg, 825 kg and 1100 kg at the 4^{th}, 3^{rd}, 2^{nd} and 1^{st} story, respectively. The structural members contribute to the story mass by approximately 250 kg at the 3^{rd}, 2^{nd} and 1^{st} story and 200 kg at the 4^{th} story. Based on these values, the distance between the geometric center and the center of mass for a generic floor level can be estimated, and for each floor level the projections in *x* and *y* direction of such distance are approximately equal to 0.05 m. This value of the eccentricity related to the center of mass is small compared with the dimension of the structure (i.e. 2.5 m), and thus it was made the simplified assumption of neglecting this small eccentricity in the calculations (where it is assumed that GC=CM for each floor level). The structure is proportionally damped, and each mode has a modal damping ratio of 1% (as also assumed in [31]).

At first the fully braced structure was considered (i.e. the diagonal wall braces are present in each bay and story of the external frames), which represents the baseline structure for damage diagnosis purposes (configuration a0-S described in Table 1 and Fig. 4). The structural model was excited by independent white noise inputs (with a duration of 720 s) applied in the geometric center of each floor level both in x and y directions. This excitation mimics the ambient excitation that can act on real structures and was modified with respect to the excitation considered in [31], which was applied only in one direction. The structural responses were collected at the locations and in the directions indicated by the arrows in Fig. 3 (four for each floor level). Among the different integration algorithms available in the FE code [31], the discrete-time integration method based on *lsim* MATLAB's command was selected [36]. Finally, as done in [31], 10% RMS noise was added on the simulated responses. The training data set (related to the baseline structure) was created by repeating the above-mentioned simulation (i.e. by generating the noisy responses) for a number of times equal to q=15. Then, damaged configurations were considered (i.e. configurations aI-S, aI-A, aII-S, aII-A, aIII-S, aIII-A described in Table 1 and Fig. 4), and the simulation of the noisy vibration responses was performed once for each of these configurations. The approach used in the benchmark FE code [31] for simulating damage was also adopted herein – i.e. interstory stiffness reductions were imposed on the baseline structure by removing in the model the stiffness contribution of some diagonal wall braces (at different stories and in different directions to create single and multiple damage scenarios). As indicated in Table 1, the considered configurations are formed by the story layouts shown in Fig. 4. In both layouts B and C only two braces contribute to the story stiffness in each direction (and the stiffness contribution of the other two braces was set to zero), but layout B is plan-symmetric while layout C is plan-asymmetric. It is important to underline that such layouts were specifically selected to compare symmetric- and asymmetric configurations that are characterized by the same values of the uncoupled interstory stiffness in each direction. The choice of the selected configurations was also dictated by the fact that in the benchmark FE code the braces can only be considered, in terms of stiffness contribution, as present or absent. There is not the option to reduce the stiffness

contribution of a single member [31]. Of course, due to the orientation of the column sections, it is expected that for layouts B and C the damage severity introduced in *y* direction is lower than the damage severity introduced in *x* direction.

Starting from the vibration responses simulated for the selected configurations, the proposed method for damage diagnosis based on UL+T inspection loads (see Section 3) was applied and the results were compared with the UL method (see end of Section 4.3). The output-only modal identification was performed using the Frequency Domain Decomposition (FDD) method [25,37], and, specifically, using its implementation in ARTeMIS Modal [38]. In this simulated analysis it was possible to identify all the twelve structural modes for each configuration. However, only the first five modes were considered in the damage diagnosis process to simulate a condition that one can encounter when performing an ambient vibration test in practice (in such case in fact the identified modal space is usually truncated). The natural frequencies identified for all the configurations are provided in Table 2, where the percent variations with respect to the frequencies of the undamaged structure are also presented. As expected, the frequencies of the damaged structures are lower than the ones of the undamaged structure. The mode shapes were identified at the sensor locations (Fig. 3b), and then through a coordinate transformation were defined (in terms of *x* direction-, *y* direction- and rotational components) with respect to the geometric center of each floor level (which is assumed as the center of mass). Then, modal flexibility matrices of the different configurations were assembled using the first five modes in Eq. (6). In Eq. (6) the considered mass matrix is the mass matrix of the model obtained from the FE code, but then forced to be diagonal (i.e. under the assumption of considering GC=CM, the small off-diagonal terms were considered as negligible and set equal to zero). This mimics the operation that one could perform when estimating the mass matrix of a real (instead of simulated) structure for which, based on engineering judgment, it is deducted that the center of mass is almost coincident with the geometric center. In such situation, more refined calculations like estimating a non-diagonal mass matrix are not useful since they do not bring to

substantially different values of the components of the mass-normalized mode shape vectors and modal flexibility matrices.

Fig. 5 and Table 3 present the outcome of the application of step 3 of proposed method (i.e. estimation of the positions of the centers of stiffness) for the considered configurations. In particular, Fig. 5 shows the interstory movements of the MF-based deflections due to the load $\boldsymbol{p_\theta}$ (1 kN m torques at all floor levels). Drifts in *x* direction, drifts in *y* direction and rotations are presented, respectively, in Fig. 5a, 5b, 5c, and the dashed lines reported in Fig. 5a, 5b represent, respectively, the thresholds Δu_θ^{TH} and Δv_θ^{TH} obtained using the procedure of Section 3.1. As shown in Fig. 5a, 5b, the drifts exceed the thresholds at 1st story for configuration aI-A, at 1st and 2nd story for configuration aII-A, and at 3rd story for configuration aIII-A. Thus, the performed statistical test correctly identifies the plan-asymmetric stories, and, according to the proposed approach, for such stories the values of the eccentricities (related to the center of stiffness) were determined using Eqs. (9,10). The identified values of the eccentricities are reported in Table 3, where these values are compared to the values of the eccentricities determined from the analytical model (i.e. by considering exact flexibility matrices of the building model). Some discrepancies are present between the two quantities, which are due to the uncertainties and truncation effects introduced in the simulation. However, as demonstrated by the percent errors shown in the table, such discrepancies are small. The values of the eccentricities identified for each configuration were used, according to the proposed method, to assemble the UL+T inspection loads (step 4 of Section 3), which are in turn adopted to estimate the MF-based deflections to be used for the damage diagnosis process. In the UL+T inspection loads 1 kN translational forces were considered. As an example, the MF-based deflections and related interstory drifts estimated for the baseline structure and the three plan-asymmetric configurations of the inspection stage are shown in Fig. 6 (results of Fig. 6a, 6b are obtained by applying the ULx+T load, while results of Fig. 6c, 6d are due to the ULy+T load).

Fig. 7 shows the statistical z index tests performed for damage detection/localization on the considered configurations, where the results of the proposed UL+T method (Fig. 7b, 7d) are compared

with the results of the existing UL method (Fig. 7a, 7c). Fig. 7a, 7b are related to the analysis performed in *x* direction, while Fig. 7c, 7d are related to the *y* direction. The dashed line reported in each figure represents the threshold. As shown by the results, both the UL+T and UL methods correctly localize the damaged stories in both directions (i.e. the 1st story for configurations aI-S, aI-A, aII-S, aII-A; the 2nd story for configurations aII-S, aII-A; the 3rd story for configurations aIII-S, aIII-A). From Fig. 7b and 7d it can be observed by considering, for example, the results for configuration aIII-A that the damage imposed at one story (i.e. 3rd story in such case) does not affect the values of the damage index at the other stories. Some false positives were obtained in the analysis in *x* direction only for some configurations. In any case the values of the z index related to the false positives are slightly higher than the considered threshold and are significantly lower than the z index values related to the damaged stories. The results of Fig. 7 demonstrate that, as already discussed in Section 4.3, both the UL+T and UL methods are suitable for damage detection/localization and confirm the inequality of Eq. (36), which was deduced analytically. In fact, for the plan-asymmetric configurations the values of z index obtained with the UL method are higher than the corresponding values determined using the UL+T method. For example, for configuration aI-A the z index at 1st story due to the ULx load is $z_{x,1}$= 84.9 (Fig. 7a), while the corresponding value obtained using the ULx+T load is $z_{x,1}$= 55.9 (Fig. 7b).

Fig. 8 and Tables 4, 5 present the results of the damage quantification for the stories of the considered configurations that have been identified as damaged. In particular, Fig. 8 shows the identified values of the damage severity and the related dispersion (represented in the figure in terms of average values ± 3 standard deviations). Using the same layout of Fig. 7, the results of Fig. 8 are presented both for the UL+T and UL methods and for the analyses both in *x* and *y* directions. In Fig. 8, points indicated with a blue circle are related to plan-symmetric stories, while points marked with a red cross are related to plan-asymmetric stories. The dashed lines in Fig. 8 indicate the reference value of the damage severity evaluated from the analytical model, adopted for the simulation (i.e. the relative portion of the uncoupled story stiffness of baseline structure in each direction that was

removed to simulate the damage). As shown in Fig. 8, for the plan-asymmetric stories the damage severity evaluated using the UL+T method is lower than the damage severity evaluated using the UL method (thus confirming the inequality of Eq. 41, which was analytically deduced in Section 4.3). However, the important result to be highlighted is that, for the plan-asymmetric stories, only the proposed UL+T method is able to provide values of the damage severity which are close to the reference values. On the contrary, the damage severities obtained for the plan-asymmetric stories using the existing UL method are in general overestimated. This important point is also confirmed by the results shown in Tables 4, 5, where (for the *x* and *y* directions, respectively) the average values of damage severity identified for the plan-asymmetric stories are compared to the reference values obtained from the analytical model, by evaluating the percent errors. As shown in these tables, the errors on damage severity obtained using the UL+T method are significantly lower than the errors related to the UL method. Considering again Fig. 8, it is worth noting that of course the damage severity for the plan-symmetric stories is equal both for the UL and UL+T methods. In addition, as expected for the selected layouts of damaged configurations (Fig. 4), when considering the UL+T method the damage severity estimated for the plan-asymmetric stories is similar to the one related to the plan-symmetric stories. Finally, it can be observed in Fig. 8 that the dispersion on the estimated values of damage severity in *y* direction is higher than the corresponding one in *x* direction. This is a consequence of the fact that the damage severity in *y* direction is lower than the one in *x* direction, and the validity of this interpretation (also confirmed by the experimental results shown in Section 5.2) is demonstrated and discussed more in detail in Appendix A.

5.1.1 Application of the proposed method on the simulated data of a multi-setup OMA test

This section presents the results of a numerical simulation that was performed to show the applicability of the proposed damage detection method starting from the data of a multi-setup OMA test executed using a limited number of sensors. The vibration data were simulated using the same FE code, the same structural model, and the same ambient excitation that were considered in previous section. However, the number of considered sensors is half of the number of sensors used in previous

section. In this simulation the data were acquired in three different setups with different layouts of the sensors (as shown in Fig. 9), differently from the previous simulation where a single setup was considered (Fig. 3). As shown in Fig. 9, sensors from 5 to 8 are reference sensors located at the top story, with fixed positions in the different setups. Sensors from 1 to 4 are roving sensors, and they were moved from one story to the other in the simulation. The simulation of the multi-setup OMA test was performed for the baseline structure (i.e. configuration a0-S) and for the damaged configuration aIII-A. The duration of the vibration responses in each setup of the multi-setup test is equal to the duration considered in the single-setup test, thus the amount of data in the multi-setup test is three times as large as the one in the single-setup test.

The mode shape components identified from the data of the different setups were merged by normalizing the components identified from the reference sensors to unity, and then the proposed method for damage diagnosis was applied. Table 6 shows the values of eccentricity identified for configuration aIII-A from the multi-setup test. The values of eccentricity obtained from the multi-setup and single-setup tests are comparable. Moreover, for both the multi-setup and single-setup tests (configuration aIII-A) the errors on the eccentricities evaluated with respect to the analytical model are of the same order (as shown in Tables 3 and 6). Fig. 10 shows the values of the z index for damage detection/localization obtained according to the proposed method for configuration aIII-A, and the results of the multi-setup and single-setup tests are compared. As shown in the figure, in the multi-setup test the 3rd story of configuration aIII-A is correctly identified as damaged, which is the same outcome obtained from the single-setup test. It is worth noting that, especially for the analysis in *y* direction, the values of z index obtained at 3rd story from the two tests (i.e. multi-setup and single-setup tests) show some differences. Such differences, however, do not affect the outcomes of the damage detection/localization, and are only due to the fact that the baseline damage-sensitive features identified in the two tests are characterized by slightly different amounts of dispersion and uncertainties. Table 7 shows the values of damage severity identified using the proposed method for configuration aIII-A from the multi-setup test. As shown in the table, the values identified from the

multi-setup test, the values identified from the single-setup test and the reference values obtained from the analytical model are comparable.

5.2 Experimental validation

The structure used for the experimental validation of the proposed method is shown in Fig. 11, and its geometry and the indication of the cross-sections of the structural members are provided in Fig. 12. Ambient vibration tests for damage diagnosis purposes were performed on this structure in September 2016, and it is worth mentioning that the considered structural configurations and the adopted experimental test setups are different from the ones of the tests performed by the IASC-ASCE Task Group in phase II of the benchmark studies [33-35].

The members of the structure are hot rolled steel members (grade 300W steel) and are connected through bolted connections. All the frames of the structure are formed by beams and columns with double-T sections (described in Fig. 12), while diagonal wall braces are present only in the four external frames of the structure. Such braces are threaded rods (with a diameter of 12.5 mm), which can be easily removed to reduce the interstory stiffness of the structure (thus simulating a damaged condition). In particular, as shown in Fig. 11, two rods are present in each bay and at each story of the external frames. Referring to the mass distribution, in the tested structure four steel plates are positioned at each floor level, and the masses of the plates are 342 kg, 454 kg, 454 kg and 454 kg at the 4^{th}, 3^{rd}, 2^{nd} and 1^{st} story, respectively. As shown in Fig. 12a, at each story the plates aligned to the *y* direction are located in the geometric center of the related bay. On the contrary, the plates aligned to the *x* direction are shifted towards south direction (for such plates the distance between the geometric center of the bay and the geometric center of the plate is approximately 0.15 m). For this distribution of the floor masses, the distance between the center of mass and the geometric center of the story was evaluated, and the projection in *x* direction of such distance is approximately equal to 0.065 m for each floor level. This distance is small if compared to the dimension of the side of the structure (i.e. 2.5 m), and thus in the damage diagnosis analysis it was made the simplified assumption of neglecting this small eccentricity, by considering GC=CM for each floor.

The responses of the structure under ambient vibrations were measured using 13 accelerometers. The sensors adopted in the test are force balance accelerometers (either uniaxial or triaxial accelerometers), and all sensors have a sensitivity of 5 V/g and a full-scale range of ±0.5g. The positions of the sensors are shown in Fig. 13, where the measured channels are indicated with black arrows. The sampling frequency selected in the data acquisition system was 1000 Hz.

At first, the AV data were acquired for the fully braced structure, i.e. configuration c0-S (described in Table 8 and Fig. 14) which represents the baseline or undamaged structure for damage diagnosis purposes (approximately 3 hours of data were recorded). Then, other configurations with braces removed from the wall bracing system were created and tested under ambient vibrations. Among all the configurations that were tested, some of them with some specific characteristics are considered for the analyses of the present paper. The considered configurations are pairs of configurations with the same number of braces removed at a certain story and in one direction, with one of each pair that has a plan-symmetric distribution of the story stiffness with respect to the considered direction, while the other of each pair is plan-asymmetric with respect to the same direction. As shown in Table 8 and by the story layouts of Fig. 14, the considered story is the 2nd story and the considered direction is the *x* direction (i.e. the west-east direction, which is the weak direction of the structure). The considered pairs of configurations are (cI-S, cI-A), (cII-S, cII-A) and (cIII-S, cIII-A), and such pairs of configurations are characterized by an increasing number of braces that were removed at 2nd story in *x* direction (i.e. two, four, and six braces removed, respectively). Configuration cIV-S with eight braces removed at 2nd story in *x* direction is also included to complete the considered progressive damage test. For the considered configurations the analyses were thus performed only in the *x* direction, and the results of the damage diagnosis process applied to the plan-symmetric configurations were considered as the reference solutions used to validate the proposed method when applied to the plan-asymmetric configurations. This validation approach was considered since, as already mentioned, the proposed method when applied to plan-symmetric configurations provides the same results of the existing PSIL method developed to perform 2D

analyses. It is worth noting that the *x* or weak direction of the structure is the preferable direction of the structure to apply the proposed method. In fact, due to the orientation of the double-T sections of columns and beams, modeling the structure with a shear-type behavior is an assumption that is much more valid for the *x* (weak) direction, rather than the *y* (strong) direction (as already observed in [28] where the data of the phase II IASC-ASCE benchmark studies are analyzed).

After the data acquisition, the measurements acquired for the baseline structure (configuration c0-S) were divided into 15 different portions of 720 s each. Such duration (i.e. 720 s) is also the duration of the measurements considered in the analyses for each configuration related to the inspection phase. Then, the acquired vibration signals were downsampled from 1000 to 100 Hz and detrended, and, as already done in the numerical simulation, the output-only modal identification was performed using the FDD method [25,37] implemented in ARTeMIS Modal [38]. According to the FDD method, the modes of the structure were manually identified by analyzing the peaks in the plot of the singular values (SV) computed from the cross spectral density matrix (an example of such plot is provided in Fig. 15 for configuration c0-S). On average, for all the configurations it was possible to identify about ten peaks of the related SV plot that can be associated to structural modes. However, only the first five modes were considered for carrying out the damage diagnosis process according to the proposed method. This choice was motivated by the fact that in the modal validation it was observed that the high-order modes are characterized by higher values of the Modal Complexity Factor [25,38] and thus by more uncertainties than the low-order modes. Referring to configuration c0-S, the considered low-order modes correspond to the first five peaks in the SV plot (Fig. 15), where it is evident that such peaks are the highest peaks in the considered frequency range. The natural frequencies of the modes identified for all the considered structural configurations are provided in Table 9. Then, under the same assumption made in the numerical simulation (i.e. considering GC=CM at each floor level), the mode shapes identified at sensor locations were evaluated with respect to the geometric center. The mass matrix of the structure was estimated based on the available

information (i.e. a $3n \times 3n$ mass matrix, assumed diagonal), and the modal flexibility matrices were assembled for all the tested configurations.

Step 3 of the proposed method was applied to identify the plan-asymmetric configurations and to estimate the values of the eccentricities $e_{y,j}$ for all the stories of the considered configurations. To this purpose, Fig. 16 shows the interstory drifts in x direction and the interstory rotations of the MF-based deflections evaluated for the load $\boldsymbol{p_\theta}$ (1 kN m torques at all floor levels). As shown in Fig. 16a, the drifts exceed the thresholds Δu_θ^{TH} (dashed lines) at 2nd story for configurations cI-A, cII-A and cIII-A. Thus, the executed statistical test correctly identifies the stories of the considered configurations that are plan-asymmetric with respect to the x direction, and the values of the eccentricities were then estimated using Eq. (9) – i.e. $e_{y,2}$ = 0.563 m, $e_{y,2}$ = 1.092 m and $e_{y,2}$ = 0.719 m at 2nd story for configurations cI-A, cII-A and cIII-A, respectively. It is worth noting that a few false positives can be observed in Fig. 16a. Such false positives were not observed, on the contrary, in the numerical simulation (as shown in Fig. 5), and can be due to more uncertainties present in the experimental test. For such few false positives some spurious eccentricities are identified, and some additional spurious torques are introduced in the inspection loads. In any case such additional spurious torques are applied to plan-symmetric stories, and thus they do not affect the outcomes of the damage diagnosis method (as shown by the results presented in this section). After having identified the values of the eccentricities $e_{y,j}$ for all the configurations, the MF-based deflections due to the inspection loads ULx+T were estimated and used for carrying out the damage diagnosis process (translational forces in the ULx+T loads are 1 kN). The components in x direction of the MF-based deflections (and the related interstory drifts) for the baseline structure (c0-S) and for the three plan-asymmetric configurations (i.e. cI-A, cII-A and cIII-A) are shown, as an example, in Fig. 17.

The results of the damage detection/localization performed for the considered structural configurations are shown in Fig. 18, where the statistical z index tests executed according to the proposed UL+T method (Fig. 18b) are compared with the statistical tests related to the existing UL method (Fig. 18a). As shown in the figure, both the UL+T and UL methods indicate that the 2nd story

is the damaged story for all the tested configurations, and thus a correct localization of the damage was obtained using both methods. It is worth mentioning that for both methods some false positives can be observed in Fig. 18 at 4th, 3rd and 1st story. However, for such false positive cases the values of the z index are slightly higher than the threshold (dashed line) and remarkably lower than the values of the z index related to the true positive cases. Finally, as already observed in the numerical simulation, the validity of the inequality expressed by Eq. (36) derived in Section 4.3 is also confirmed by the experimental results – i.e. for plan-asymmetric configurations the z index due to the UL method is higher than the z index due to the UL+T method. For example, for configuration cIII-A at 2nd story $z_{x,2}$ = 124.6 and $z_{x,2}$= 100.2 were obtained using the ULx load and the ULx+T load, respectively.

The results of the damage quantification are shown in Fig. 19, where the identified values of the damage severity and the related dispersion (i.e. average values ± 3 standard deviations) are provided both for the UL method (Fig. 19a) and the UL+T method (Fig. 19b). The values of damage severity obtained for the plan-symmetric configurations (i.e. points marked with a blue circle in the figure) can be considered as the reference solutions, as already discussed in previous paragraphs, and of course the same values were obtained using the UL+T and UL methods. Based on this premise and when considering the plan-asymmetric configurations (i.e. points indicated with a red cross), it is evident from the results that the damage severity is overestimated using the existing UL method, while only using the proposed UL+T method the correct values of the damage severity can be obtained (this is also in agreement with the inequality of Eq. 41, derived analytically). In fact, in Fig. 19b (UL+T method) the damage severities obtained for the plan-symmetric and plan-asymmetric configurations are almost coincident, and such values progressively increase when considering an increasing number of braces removed from the wall bracing system. The comparison between the damage quantification results of the UL+T and UL methods is also shown in Table 10, specifically by presenting the percent errors that affect the average values of damage severity identified for the plan-asymmetric configurations. Such errors were evaluated with respect to the reference solutions

obtained for the corresponding plan-symmetric configurations. As shown in the table, the errors on the damage severity estimated with the UL+T method are remarkably lower than the UL errors. Considering again Fig. 19, it is evident that the dispersion on the estimated values of damage severity decreases with the increase of the amount of the damage (as already observed in the numerical simulation and as discussed more in detail in Appendix A). Referring to the amounts of damage introduced in the tested configurations and estimated using the proposed damage diagnosis method, it is important to underline that the considered damaged configurations are characterized by values of the damage severity that correspond in some cases to realistic situations, while other cases can be more rare in practical situations. In any case, configurations that are characterized by very high values of the damage severity (such as, for example, configuration cIV-S which was tested after removing all the braces from the 2nd story) were considered to have a complete insight of the tendencies of the damage quantification results. An estimation of the minimum amount of damage that is theoretically detectable for the performed experimental test was also carried out, according to the approach that is outlined in Appendix B. For example, for the story of the considered structure where the damage was applied (i.e. 2nd story), the minimum damage severity in x direction that is detectable using the proposed method is $\alpha_{x,2,min}$= 0.0593 (i.e. the minimum detectable interstory stiffness reduction is 5.93%). Such value is comparable and similar to the values of minimum detectable damage severity obtained in previous researches where the existing PSIL method was applied on planar full-scale shear buildings (as shown, for example, in [11]).

5.2.1 Sensitivity of the damage diagnosis process to potential errors in the estimation of the mass matrix

In the proposed method, similarly to the existing PSIL method [9], an a-priori estimate of the system mass matrix is used, and this could be a potential source of errors for the overall damage diagnosis process. This section presents a study that was performed to investigate the sensitivity of the process to potential errors in the estimation of the mass matrix. The study was conducted by considering the steel frame structure tested under ambient vibrations, and the proposed method was applied by

introducing systematic perturbations on the components of the mass matrix considered in the previous section. In particular, each *j*-th story mass of the structure was perturbed by ±10%, ±20%, ±30%, ±40%, ±50%, and the calculations were repeated for all the stories (i.e. for *j*=1…*n*, where *n*=4). This study was performed for all the tested plan-asymmetric configurations (i.e. cI-A, cII-A, cIII-A). It is worth noting that the imposed amounts of mass perturbations are equal to the ones used in a mass-sensitivity study presented in [39].

Table 11 shows the values of eccentricity identified in presence of mass perturbations for configuration cI-A (i.e. the one with the lower amount of imposed damage), together with the percent variations evaluated with respect to the eccentricity obtained with no mass perturbations. As shown in the table, the maximum of the absolute error on the eccentricities is 1.2%. By performing the same analysis for the other configurations, it was found that the maximum errors on the eccentricities are 0.5% and 1.0% for configurations cII-A and cIII-A, respectively. Fig. 20 shows the effects of the mass perturbations on the z index statistical tests for damage detection/localization, by considering, as an example, configuration cI-A with mass perturbations applied at 2nd story (Fig. 20a) and at 4th story (Fig. 20b). It can be observed in the figure, that even in the worst-case scenario (i.e. ±50% mass perturbations) the outcomes of the statistical tests are unaltered, and the damage is correctly localized at 2nd story. Table 12 shows the values of damage severity identified in presence of mass perturbations for configuration cI-A and the percentages of their variations evaluated with respect to the damage severity obtained with no mass perturbations. As shown in the table, the maximum of the absolute error on the damage severity is 1.6%. The same analysis performed for configurations cII-A and cIII-A showed that the maximum errors on the damage severity for such configurations are 3.6% and 1.9%, respectively. Overall, it was thus found that the sensitivity of the proposed damage diagnosis process to the considered mass perturbations is low.

The case of mass perturbations that are uniform along the height of the structure (thus not applied at each single story, as discussed earlier) was also analyzed, and the results showed that the proposed method is insensitive to such kind of mass perturbations. This is because a uniform scaling

on the mass matrix of the structure generate a uniform scaling on the modal flexibility matrices, deflections and interstory drifts (as demonstrated in [14]), and the damage indices of the proposed method (i.e. z and damage severity indices) are not altered if all the damage-sensitive features (both in the baseline and possibly damaged states) are multiplied by the same scalar.

6 Conclusions

In this paper, a method that uses modal flexibility-based deflections for performing a vibration-based damage diagnosis in building structures tested under ambient vibrations is proposed. The proposed method can be used for detecting, localizing and quantifying the damage, and it is applicable for simple rectangular plan-symmetric "box type" 3D building structures which may experience asymmetric damage. The method is an extension of the existing PSIL method developed for planar structures (both in the baseline and possibly damaged states).

The effectiveness of the proposed method was verified, on one side, by performing numerical analyses. On the other side, experimental ambient vibration tests were performed on a one-third scale building structure, and then the acquired data were processed using the proposed approach. In both cases the considered structure is a four-story two-bay by two-bay steel frame structure, and diagonal braces were removed from the wall bracing system of the structure to impose stiffness reductions and to create the damaged configurations. Both the numerical and experimental analyses demonstrated that the proposed method is able to perform the damage diagnosis process, by identifying the stories and directions of the structure affected by the damage and by providing an estimate of the damage severity. In both cases this result was achieved starting from noisy vibration data (either simulated or real data) and by considering a limited number of identified structural modes. It was also demonstrated that the proposed method is applicable in the case of multi-setup OMA tests executed with a limited number of sensors. Moreover, the results of a performed mass-sensitivity study showed that the proposed method is robust against potential errors in the estimation of the mass matrix of the structure.

The proposed method based on the use of UL+T inspection loads was also compared with a more simplified procedure that provides the same results of the existing PSIL method, developed for planar structures. This simplified procedure is based on the use of UL loads, and the comparison was done both in the numerical and experimental analyses. Referring to the damage detection/localization, it was observed that, even if the values of the z index obtained by applying UL loads to plan-symmetric buildings with asymmetric damage are different from the ones estimated for UL+T loads, the overall performance of the simplified method is comparable to the one of the more complex proposed method. This is not true when the damage quantification problem is considered. For plan-symmetric buildings with asymmetric damage, in fact, the proposed method provides correct values of the damage severity, while the simplified method systematically overestimates such quantities. Ultimately, it was thus demonstrated that, among the two methods, only the proposed one can be used to perform a correct and complete damage diagnosis process in plan-symmetric buildings with asymmetric damage.

Declaration of competing interest

The authors declare that they have no known competing financial interests or personal relationships that could have appeared to influence the work reported in this paper.

Acknowledgments

The authors wish to thank all the people that provided information about the tested building structure and/or assistance during the ambient vibration tests performed at the EERF laboratory of UBC (Vancouver), especially Martin Turek and Yuxin Pan. The use of the MATLAB-based finite element analysis code developed by the IASC-ASCE Task Group (phase I) is gratefully acknowledged.

Appendix A. Observations on the estimated values of damage severity and related dispersion

Both in the numerical and experimental analyses it was observed that the dispersion on the estimated values of damage severity is higher for the stories that are characterized by the lower values of damage severity (as shown in Figs. 8, 19). To explain this observed result, let us consider the following simplified interpretation and let us evaluate (starting from Eq. 15) how a perturbation imposed on the

average value of the drift related to the baseline structure affects the value of the damage severity. By considering, for instance, the analysis in x direction, the perturbed value of the damage severity can be expressed as follows

$$\tilde{\alpha}_{x,j} = \frac{\Delta u_{I,x,j} - \Delta \tilde{u}_{B,x,j}}{\Delta u_{I,x,j}} = \frac{\Delta u_{I,x,j} - [\Delta \bar{u}_{B,x,j} + 1\, s(\Delta u_{B,x,j})]}{\Delta u_{I,x,j}} \quad \text{(A1)}$$

where the perturbed value of the drift related to the baseline structure $\Delta \tilde{u}_{B,x,j}$ is obtained by adding one standard deviation to the average value of such quantity. Eq. (A1) can then be rearranged as follows to express the perturbed value of damage severity as a function of the unperturbed value of damage severity $\alpha_{x,j}$ (i.e. Eq. 15)

$$\tilde{\alpha}_{x,j} = \frac{\Delta u_{I,x,j} - \Delta \bar{u}_{B,x,j}}{\Delta u_{I,x,j}} \left(1 - \frac{1\, s(\Delta u_{B,x,j})}{\Delta u_{I,x,j} - \Delta \bar{u}_{B,x,j}}\right) = \alpha_{x,j}\,(1 - c_1) \quad \text{(A2)}$$

where a coefficient c_1 with the following expression has been introduced

$$c_1 = \frac{1\, s(\Delta u_{B,x,j})}{\Delta u_{I,x,j} - \Delta \bar{u}_{B,x,j}} \quad \text{(A3)}$$

The numerator in the above expression is independent from the amount of damage, while the denominator is a positive quantity that increases when considering increasing values of the damage severity present in the j-th story. This implies that, for increasing values of the damage severity, the coefficient c_1 decreases tending to 0 and the term (1 - c_1) of Eq. (A2) increases tending to 1. Thus, for increasing amount of damage, the perturbed and unperturbed values of the damage severity in Eq. (A2) get closer, which means, in other words, that, for increasing amount of damage, the dispersion on the estimated damage severity is lower.

Appendix B. Evaluation of the minimum detectable damage severity

The estimation of the minimum damage severity that is theoretically detectable was performed by adapting the approach presented in [11] (where the existing PSIL method was applied on planar shear buildings) to the case of the proposed UL+T method and of the analyses presented in this paper. By considering, for instance, the analysis in x direction, the following steps were performed. After having estimated the interstory drifts of the j-th story of the baseline structure due to the ULx+T inspection

load and their statistical properties, the minimum drift for which the *j*-th story of the structure is classified as damaged was determined as follows

$$\Delta u_{I,x,j,min} = \Delta \bar{u}_{B,x,j} + z^{TH}\, s\left(\Delta u_{B,x,j}\right) \tag{B1}$$

which is an expression that can be derived by rearranging Eq. (14). Finally, the minimum value of the damage severity that can be detected at the *j*-th story of the structure was estimated as follows

$$\alpha_{x,j,min} = \frac{\Delta u_{I,x,j,min} - \Delta \bar{u}_{B,x,j}}{\Delta u_{I,x,j,min}} \tag{B2}$$

which is an expression that can be derived from Eq. (15), by simply considering the drift estimated using Eq. (B1) as the drift related to the inspection phase in Eq. (15). It is important to underline that if the dispersion on the interstory drifts in the baseline state increases (e.g. due to increased uncertainties in the damage diagnosis process), then higher values of the minimum detectable damage severity are obtained. This principle can be shown by substituting Eq. (B1) into Eq. (B2) and by rearranging the derived expression, as follows

$$\alpha_{x,j,min} = \frac{z^{TH}\, s\left(\Delta u_{B,x,j}\right)}{\Delta \bar{u}_{B,x,j} + z^{TH}\, s\left(\Delta u_{B,x,j}\right)} = \frac{1}{\frac{\Delta \bar{u}_{B,x,j}}{z^{TH}\, s\left(\Delta u_{B,x,j}\right)} + 1} \tag{B3}$$

From Eq. (B3) it is evident that, when considering the parameters $\Delta \bar{u}_{B,x,j}$ and z^{TH} as fixed, an increase in the standard deviation of the drifts of the baseline structure $s\left(\Delta u_{B,x,j}\right)$ leads to an increase in the minimum detectable damage severity $\alpha_{x,j,min}$.

References

[1] Sohn H, Farrar CR, Hemez FM, Shunk DD, Stinemates DW, Nadler BR, Czarnecki JJ. A Review of Structural Health Monitoring Literature: 1996-2001. Report LA-13976-MS, Los Alamos National Laboratory, Los Alamos, NM, USA; 2003.

[2] Figueiredo E, Park G, Figueiras J, Farrar C, Worden K. Structural Health Monitoring Algorithm Comparisons Using Standard Data Sets. Report LA-14393 Los Alamos National Laboratory, Los Alamos, New Mexico, USA, March 2009.

[3] Farrar CR, Worden K. Structural health monitoring: A machine learning perspective. 1st ed. Chichester, UK: John Wiley & Sons; 2013.

[4] Cunha A, Caetano E, Magalhães F, Moutinho C. Recent perspectives in dynamic testing and monitoring of bridges. Structural Control and Health Monitoring 2013; 20:853–877.

[5] Koo KY, Lee JJ, Yun CB, Kim JT. Damage detection in beam-like structures using deflections obtained by modal flexibility matrices. Smart Structures and Systems 2008;4(5):605–28.

[6] Koo KY, Lee JJ, Yun CB. Damage detection of bridge structures using modal flexibility under temperature variations. IFAC Proceedings Volumes – 17th IFAC World Congress 2008;41(2):15762–7.

[7] Sung SH, Jung HJ, Jung HY. Damage detection for beam-like structures using the normalized curvature of a uniform load surface. Journal of Sound and Vibration 2013;332(6):1501–19.

[8] Catbas FN, Brown DL, Aktan AE. Use of modal flexibility for damage detection and condition assessment: Case studies and demonstrations on large structures. Journal of Structural Engineering 2006; 132 (11): 1699-1712.

[9] Koo KY, Sung SH, Park JW, Jung HJ. Damage detection of shear buildings using deflections obtained by modal flexibility. Smart materials and structures 2010; 19 (11): 115026.

[10] Koo KY, Sung SH, Jung HJ. Damage quantification of shear buildings using deflections obtained by modal flexibility. Smart materials and structures 2011; 20 (4): 045010.

[11] Sung SH, Koo KY, Jung HY, Jung HJ. Damage-induced deflection approach for damage localization and quantification of shear buildings: validation on a full-scale shear building. Smart materials and structures 2012; 21 (11): 115013.

[12] Zhang J, Xu JC, Guo SL, Wu ZS. Flexibility-based structural damage detection with unknown mass for IASC-ASCE benchmark studies. Engineering Structures 2013; 48: 486–496.

[13] Bernagozzi G, Ventura CE, Allahdadian S, Kaya Y, Landi L, Diotallevi PP. Application of modal flexibility-based deflections for damage diagnosis of a steel frame structure. In: Vestroni F,

Gattulli V, Romeo F (editors), Procedia Engineering, X International Conference on Structural Dynamics EURODYN 2017, volume 199, pp. 2026-2033.

[14] Bernagozzi G, Mukhopadhyay S, Betti R, Landi L, Diotallevi PP. Output-only damage detection in buildings using proportional modal flexibility-based deflections in unknown mass scenarios. Engineering Structures 2018; 167: 549-566.

[15] Pandey AK, Biswas M. Damage Detection in Structures Using Changes in Flexibility. Journal of Sound and Vibration 1994; 169 (1): 3-17.

[16] Bernal D, Gunes B. Flexibility Based Approach for Damage Characterization: Benchmark Application. Journal of Engineering Mechanics 2004; 130(1): 61-70.

[17] Zhao J, DeWolf J. Sensitivity Study for Vibrational Parameters Used in Damage Detection. Journal of Structural Engineering 1999; 125 (4): 410-416.

[18] Zhang Z, Aktan AE. Application of Modal Flexibility and Its Derivatives in Structural Identification. Research in Nondestructive Evaluation 1998; 10 (1): 43-61.

[19] Wang Y, Thambiratnam DP, Chan THT, Nguyen A. Method development of damage detection in asymmetric buildings. Journal of Sound and Vibration 2018; 413; 41-56.

[20] Wang Y, Thambiratnam DP, Chan THT, Nguyen A. Damage detection in asymmetric buildings using vibration-based techniques. Structural Control & Health Monitoring 2018; 25: e2148.

[21] Wang JF, Lin CC, Lin GL, Yang CH. Story Damage Identification of Irregular Buildings Based on Earthquake Records. Earthquake Spectra 2013; 29 (3): 963–985.

[22] Wang JF, Lin CC, Yen SM. A story damage index of seismically-excited buildings based on modal frequency and mode shape. Engineering Structures 2007; 29 (9): 2143-2157.

[23] Stubbs N, Kim JT, Topole K. An efficient and robust algorithm for damage localization in offshore structures. Proceedings of the 10th ASCE Structures Conference, American Society of Civil Engineers, New York, NY, 1992, pp. 543–546.

[24] Stubbs N, Kim JT, Farrar C. Field verification of a nondestructive damage localization and severity estimation algorithm. Proceedings of the 13th International Modal Analysis Conference (IMAC), Nashville, TN, 1995, pp. 210–218.

[25] Brincker R, Ventura C. Introduction to OPERATIONAL MODAL ANALYSIS. 1st ed. Chichester, UK: John Wiley & Sons; 2015.

[26] Bernal D. Modal scaling from known mass perturbations. Journal of Engineering Mechanics 2004; 130 (9): 1083 -1088.

[27] López-Aenlle M, Fernández P, Brincker R, Fernández-Canteli A. Scaling-factor estimation using an optimized mass-change strategy. Mechanical Systems and Signal Processing 2010; 24 (5):1260-1273.

[28] Bernagozzi G, Landi L, Diotallevi PP. Truncation error analysis on modal flexibility-based deflections: application to mass regular and irregular structures. Engineering Structures 2017; 142: 192–210.

[29] Barnett V, Lewis T. Outliers in statistical data. 3rd ed. Chichester (UK): John Wiley & Sons; 1994.

[30] Balsamo L, Betti R. Data-based structural health monitoring using small training data sets. Structural Control & Health Monitoring 2015; 22 (10): 1240-1264.

[31] Johnson EA, Lam HF, Katafygiotis LS, Beck JL. Phase I IASC-ASCE Structural Health Monitoring Benchmark Problem Using Simulated Data. Journal of Engineering Mechanics 2004; 130 (1): 3-15.

[32] Luş H¸ Betti R, Yu J, De Angelis M. Investigation of a System Identification Methodology in the Context of the ASCE Benchmark Problem. Journal of Engineering Mechanics 2004; 130:71-84.

[33] Dyke SJ, Bernal D, Beck J, Ventura CE. An experimental benchmark problem in structural health monitoring. In: Chang FK (editor), Structural Health Monitoring: The Demand and Challenges -

Proceedings of the 3rd International Workshop in Structural Health Monitoring, CRC Press, Boca Raton, FL, 2001, pp. 488-497.

[34] Ventura CE, Lord JF, Turek M, Sereci AM, Radulescu D, Radulescu C. Experimental Studies and Remote Monitoring of IASC-ASCE Benchmark Test Frame. Proceedings of the 21st International Modal Analysis Conference (IMAC), Orlando, FL, USA, February 3–6, 2003.

[35] Dyke SJ, Bernal D, Beck J, Ventura C. Experimental Phase II of the Structural Health Monitoring Benchmark Problem. Proceedings of the 16th ASCE Engineering Mechanics Conference, Seattle, Washington, USA, July 16-18, 2003.

[36] MATLAB. Natick, Massachusetts, United States: The MathWorks Inc.

[37] Brincker R, Zhang L, Andersen P. Modal identification of output-only systems using frequency domain decomposition. Smart Materials and Structures 2001; 10 (3): 441-445.

[38] ARTeMIS Modal software, Structural Vibration Solutions, http://www.svibs.com/

[39] Omrani R, Hudson RE, Taciroglu E. Story-by-story estimation of the stiffness parameters of laterally-torsionally coupled buildings using forced or ambient vibration data: II. Application to experimental data. Earthquake Engineering & Structural Dynamics 2012; 41:1635–1649.

LIST OF TABLES

Configuration	State	Type	Description*
a0-S	Undamaged	Plan - symmetric	Layout A at all stories
aI-S	Damaged	Plan - symmetric	Layout B at 1st story; layout A at other stories
aI-A	Damaged	Plan - asymmetric	Layout C at 1st story; layout A at other stories
aII-S	Damaged	Plan - symmetric	Layout B at 1st and 2nd story; layout A at other stories
aII-A	Damaged	Plan - asymmetric	Layout C at 1st and 2nd story; layout A at other stories
aIII-S	Damaged	Plan - symmetric	Layout B at 3rd story; layout A at other stories
aIII-A	Damaged	Plan - asymmetric	Layout C at 3rd story; layout A at other stories

* the layouts A, B, C are described in Fig. 4

Table 1. Configurations considered in the numerical simulation with description of damage scenarios.

Configuration	Natural frequency f_i [Hz] (% variation w.r.t. baseline structure)				
	1st mode	2nd mode	3rd mode	4th mode	5th mode
a0-S	9.08	11.33	15.82	24.51	30.66
aI-S	8.01 (-11.8)	10.55 (-6.9)	14.26 (-9.9)	22.66 (-7.6)	29.30 (-4.5)
aI-A	7.32 (-19.4)	10.25 (-9.5)	14.06 (-11.1)	22.46 (-8.4)	29.20 (-4.8)
aII-S	7.52 (-17.2)	10.16 (-10.3)	13.48 (-14.8)	21.97 (-10.4)	28.81 (-6.0)
aII-A	6.64 (-26.9)	9.77 (-13.8)	13.87 (-12.3)	20.51 (-16.3)	28.22 (-8.0)
aIII-S	8.69 (-4.3)	11.04 (-2.6)	15.23 (-3.7)	22.27 (-9.2)	29.10 (-5.1)
aIII-A	8.40 (-7.5)	10.94 (-3.4)	14.84 (-6.2)	21.58 (-12.0)	28.81 (-6.0)

Table 2. Identified natural frequencies of the configurations considered in the numerical simulation.

Case	Eccentricities from analytical model (reference values)		Identified eccentricities			
	$e_{y,REF}$ (m)	$e_{x,REF}$ (m)	$e_{y,ID}$ (m)	Error (%)	$e_{x,ID}$ (m)	Error (%)
aI-A 1st story	0.688	0.365	0.732	6.3	0.383	4.7
aII-A 1st story	0.688	0.365	0.754	9.6	0.390	6.7
aII-A 2nd story	0.688	0.365	0.719	4.5	0.358	-1.9
aIII-A 3rd story	0.688	0.365	0.621	-9.8	0.346	-5.4

Table 3. Identified eccentricities for the plan-asymmetric configurations considered in the numerical simulation and related errors (evaluated w.r.t. to the reference values obtained from the analytical model).

Case	Damage severity α_x from analytical model (reference values)	Identified results			
		Existing UL method (*x* dir.)		Proposed UL+T method (*x* dir.)	
		Damage severity	Error (%)	Damage severity	Error (%)
aI-A 1st story	0.355	0.470	32.2	0.368	3.7
aII-A 1st story	0.355	0.470	32.2	0.363	2.1
aII-A 2nd story	0.355	0.460	29.5	0.371	4.6
aIII-A 3rd story	0.355	0.444	25.1	0.366	2.9

Table 4. Errors on the values of the damage severity (α_x) in *x* direction obtained for the plan-asymmetric configurations (numerical simulation): comparison between the proposed UL+T method and the existing UL method.

Case	Damage severity α_y from analytical model (reference values)	Identified results			
		Existing UL method (*y* dir.)		Proposed UL+T method (*y* dir.)	
		Damage severity	Error (%)	Damage severity	Error (%)
aI-A 1st story	0.226	0.287	27.0	0.218	-3.7
aII-A 1st story	0.226	0.279	23.2	0.204	-10.0
aII-A 2nd story	0.226	0.273	20.7	0.213	-5.7
aIII-A 3rd story	0.226	0.284	25.4	0.229	1.4

Table 5. Errors on the values of the damage severity (α_y) in *y* direction obtained for the plan-asymmetric configurations (numerical simulation): comparison between the proposed UL+T method and the existing UL method.

Direction	Reference values		Results identified from multi-setup OMA		
	Eccentricity from analytical model (m)	Eccentricity identified from single-setup OMA (m)	Eccentricity (m)	Error w.r.t. analytical model (%)	Error w.r.t. single-setup OMA (%)
y direction (e_y)	0.688	0.621	0.620	-10.0	-0.2
x direction (e_x)	0.365	0.346	0.341	-6.7	-1.4

Table 6. Eccentricities identified for configuration aIII-A (3rd story) in the numerical simulation of the multi-setup OMA test.

Direction	Reference values		Results identified from multi-setup OMA		
	Damage severity from analytical model	Damage severity from single-setup OMA	Damage severity	Error w.r.t. analytical model (%)	Error w.r.t. single-setup OMA (%)
x direction (α_x)	0.355	0.366	0.369	3.8	0.9
y direction (α_y)	0.226	0.229	0.239	5.8	4.4

Table 7. Values of damage severity identified using the proposed UL+T method for configuration aIII-A (3rd story) in the numerical simulation of the multi-setup OMA test.

Configuration	State	Type	Number of braces removed (at 2nd story in *x* direction)
c0-S	Undamaged	Plan - symmetric	0
cI-S	Damaged	Plan - symmetric	2
cI-A	Damaged	Plan - asymmetric	2
cII-S	Damaged	Plan - symmetric	4
cII-A	Damaged	Plan - asymmetric	4
cIII-S	Damaged	Plan - symmetric	6
cIII-A	Damaged	Plan - asymmetric	6
cIV-S	Damaged	Plan - symmetric	8

Table 8. Configurations considered in the ambient vibration tests with description of damage scenarios.

Configuration	Natural frequency f_i [Hz] (% variation w.r.t. baseline structure)				
	1st mode	2nd mode	3rd mode	4th mode	5th mode
c0-S	7.62	8.01	15.53	21.44	22.07
cI-S	6.93 (-9.0)	7.18 (-10.4)	14.45 (-6.9)	21.34 (-0.5)	21.92 (-0.7)
cI-A	6.89 (-9.6)	7.57 (-5.5)	14.80 (-4.7)	20.90 (-2.5)	21.73 (-1.5)
cII-S	6.59 (-13.5)	6.84 (-14.6)	12.74 (-17.9)	21.34 (-0.5)	21.88 (-0.9)
cII-A	5.71 (-25.0)	7.32 (-8.5)	14.06 (-9.4)	21.29 (-0.7)	21.83 (-1.1)
cIII-S	6.06 (-20.5)	6.54 (-18.3)	11.28 (-27.4)	21.34 (-0.5)	21.88 (-0.9)
cIII-A	5.37 (-29.5)	6.93 (-13.4)	12.55 (-19.2)	21.24 (-0.9)	21.78 (-1.3)
cIV-S	4.93 (-35.3)	6.06 (-24.4)	9.13 (-41.2)	21.34 (-0.5)	21.78 (-1.3)

Table 9. Identified natural frequencies of the configurations considered in the ambient vibration tests.

No. of braces removed	Symmetric conf. *		Asymmetric configurations				
	Reference values			Existing UL method		Proposed UL+T method	
	Conf.	Damage severity	Conf.	Damage severity	Error (%)	Damage severity	Error (%)
2	cI-S	0.293	cI-A	0.362	23.3	0.314	7.2
4	cII-S	0.509	cII-A	0.655	28.6	0.500	-1.7
6	cIII-S	0.645	cIII-A	0.724	12.3	0.680	5.5
8	cIV-S	0.803					

* for the plan-symmetric configurations the UL and UL+T methods provide the same results.

Table 10. Errors on the values of the damage severity (α_x) obtained for the plan-asymmetric configurations (analysis in x direction, AV tests): comparison between the proposed UL+T method and the existing UL method.

δm_j	Eccentricity e_y (m) conf. cI-A (% variation w.r.t. $\delta m_j = 0\%$)			
	j=1	j=2	j=3	j=4
+50%	0.562 (-0.1)	0.568 (0.9)	0.563 (0.1)	0.558 (-0.8)
+40%	0.562 (-0.1)	0.567 (0.7)	0.563 (0.1)	0.559 (-0.7)
+30%	0.562 (-0.1)	0.566 (0.6)	0.563 (0.1)	0.560 (-0.5)
+20%	0.563 (0.0)	0.565 (0.4)	0.563 (0.1)	0.561 (-0.4)
+10%	0.563 (0.0)	0.564 (0.2)	0.563 (0.0)	0.562 (-0.2)
0%	0.563	0.563	0.563	0.563
-10%	0.563 (0.0)	0.562 (-0.2)	0.563 (0.0)	0.564 (0.2)
-20%	0.563 (0.1)	0.560 (-0.4)	0.563 (0.0)	0.565 (0.4)
-30%	0.563 (0.1)	0.559 (-0.6)	0.562 (-0.1)	0.566 (0.7)
-40%	0.563 (0.1)	0.558 (-0.8)	0.562 (-0.1)	0.568 (0.9)
-50%	0.564 (0.1)	0.557 (-1.1)	0.562 (-0.1)	0.570 (1.2)

Table 11. Effect of potential errors in mass matrix estimation on the eccentricity e_y (m) for configuration cI-A at 2nd story (proposed method; ambient vibration tests).

δm_j	Damage severity conf. cI-A (% variation w.r.t. $\delta m_j = 0\%$)			
	j=1	j=2	j=3	j=4
+50%	0.318 (1.1)	0.310 (-1.3)	0.313 (-0.5)	0.317 (0.7)
+40%	0.317 (0.9)	0.311 (-1.1)	0.313 (-0.4)	0.316 (0.6)
+30%	0.316 (0.7)	0.312 (-0.8)	0.313 (-0.3)	0.316 (0.5)
+20%	0.316 (0.5)	0.313 (-0.5)	0.314 (-0.2)	0.315 (0.3)
+10%	0.315 (0.3)	0.313 (-0.3)	0.314 (-0.1)	0.315 (0.2)
0%	0.314	0.314	0.314	0.314
-10%	0.314 (-0.3)	0.315 (0.3)	0.315 (0.1)	0.314 (-0.2)
-20%	0.313 (-0.5)	0.316 (0.6)	0.315 (0.3)	0.313 (-0.4)
-30%	0.312 (-0.7)	0.317 (0.9)	0.316 (0.4)	0.313 (-0.6)
-40%	0.311 (-1.0)	0.318 (1.2)	0.316 (0.6)	0.312 (-0.8)
-50%	0.310 (-1.2)	0.319 (1.6)	0.317 (0.8)	0.311 (-1.1)

Table 12. Effect of potential errors in mass matrix estimation on the damage severity α_x for configuration cI-A at 2nd story (proposed method; ambient vibration tests).

LIST OF FIGURES

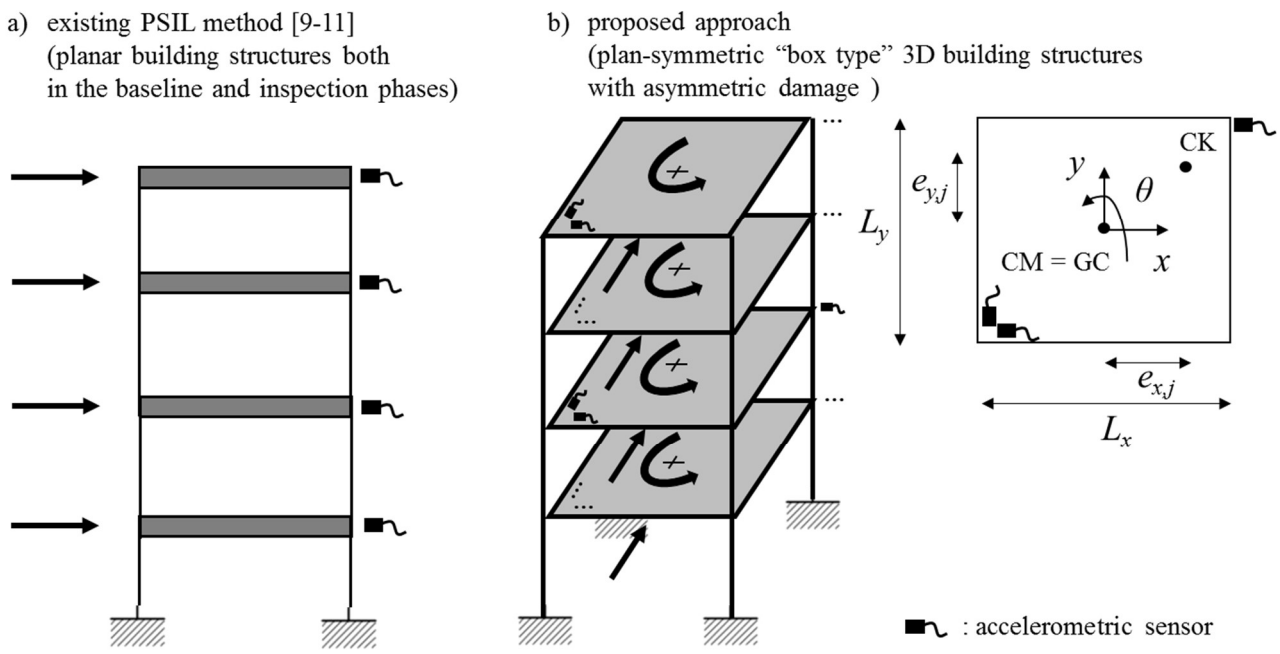

Figure 1. Types of structures and inspection loads considered in the different approaches: a) existing PSIL method [9-11]; b) proposed approach.

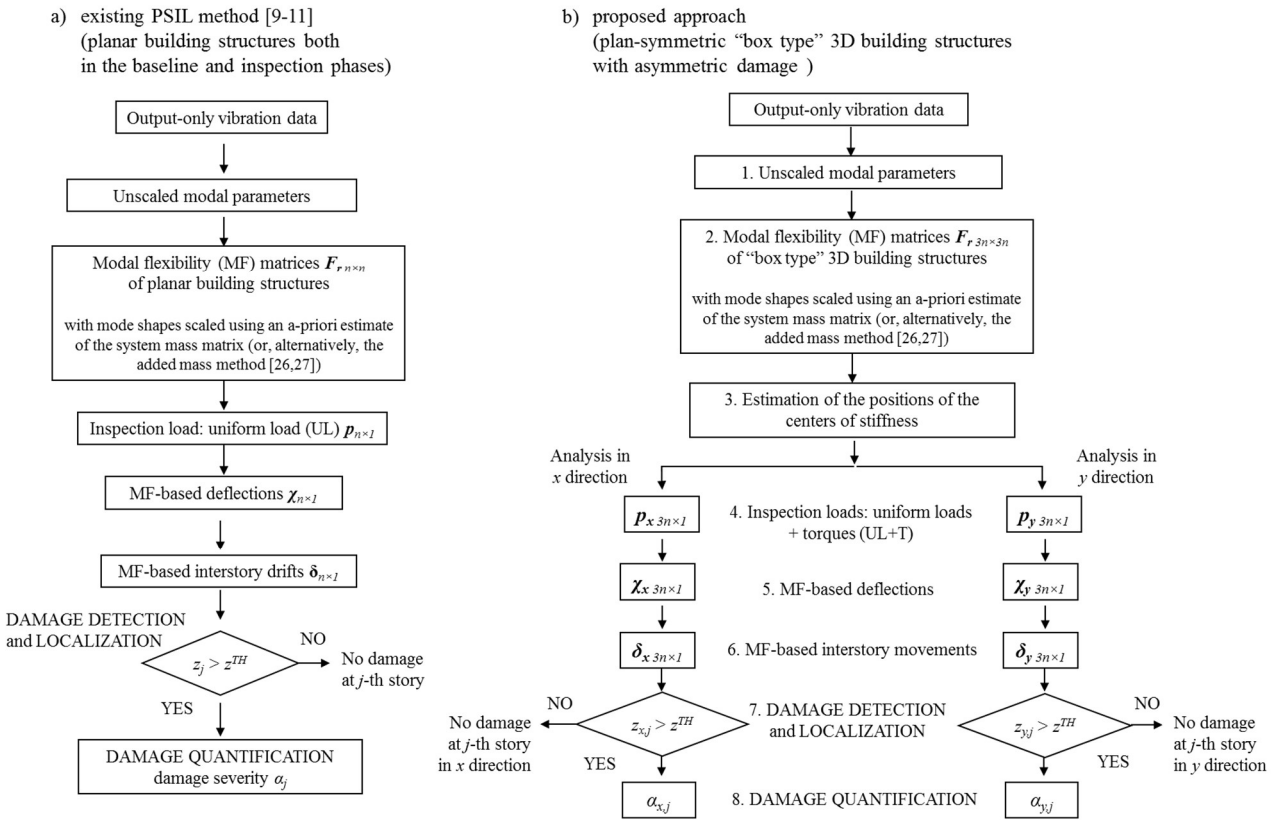

Figure 2. Flow chart of the methods: a) existing PSIL method [9-11]; b) proposed approach.

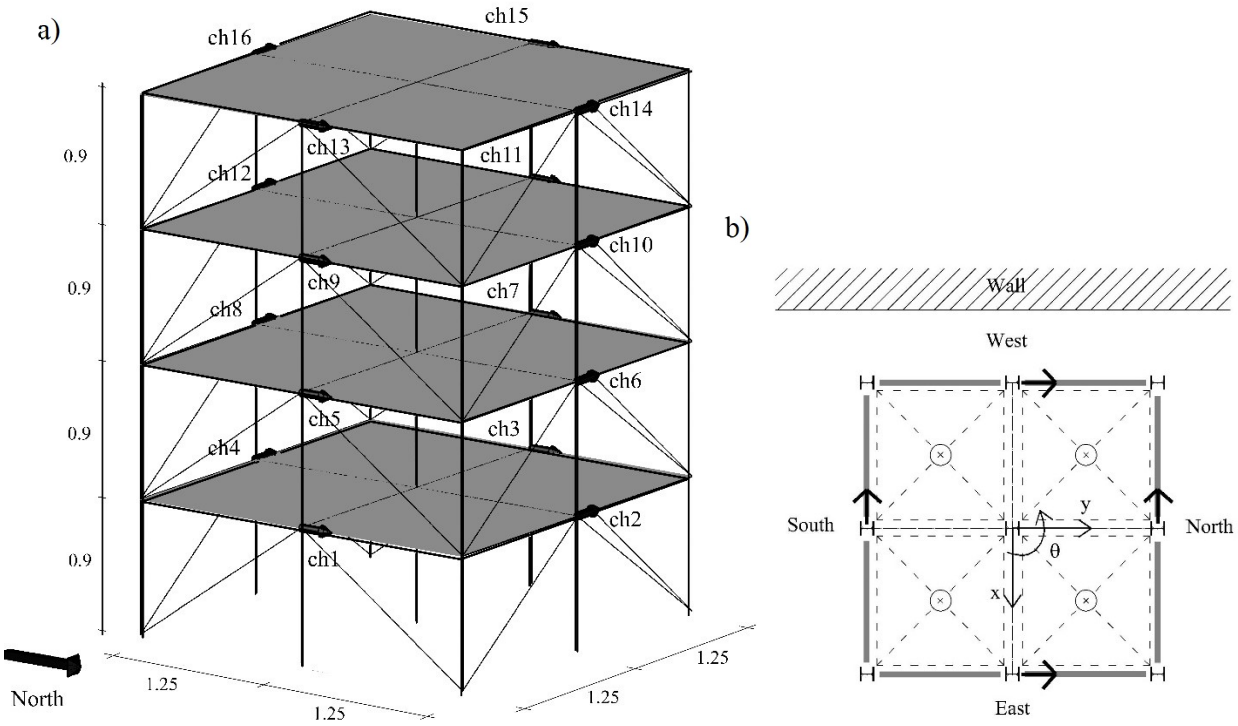

Figure 3. Degrees-of-freedom of the frame structure measured in the numerical simulation (dimensions in m): a) 3D view; b) plan view.

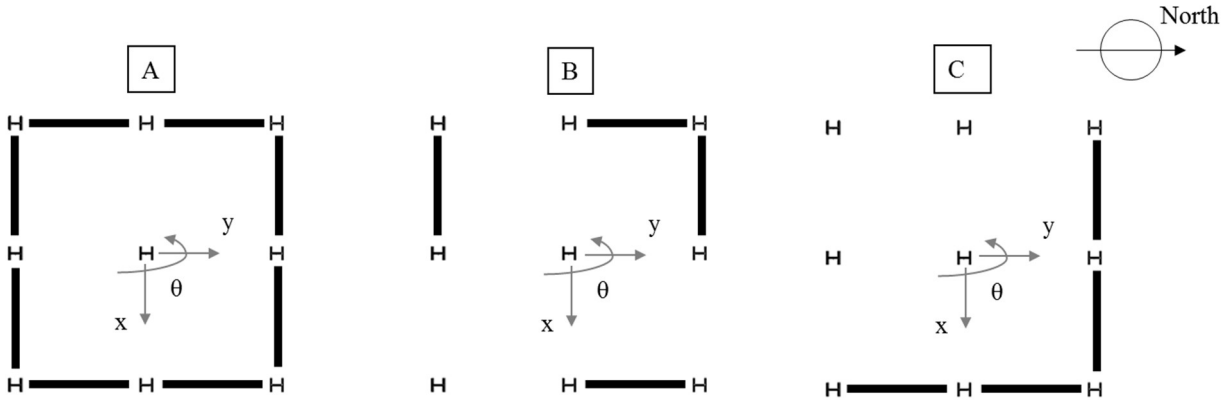

Figure 4. Schematic plan view of the story layouts A, B, C (used in Table 1 to describe the configurations considered in the numerical simulation).

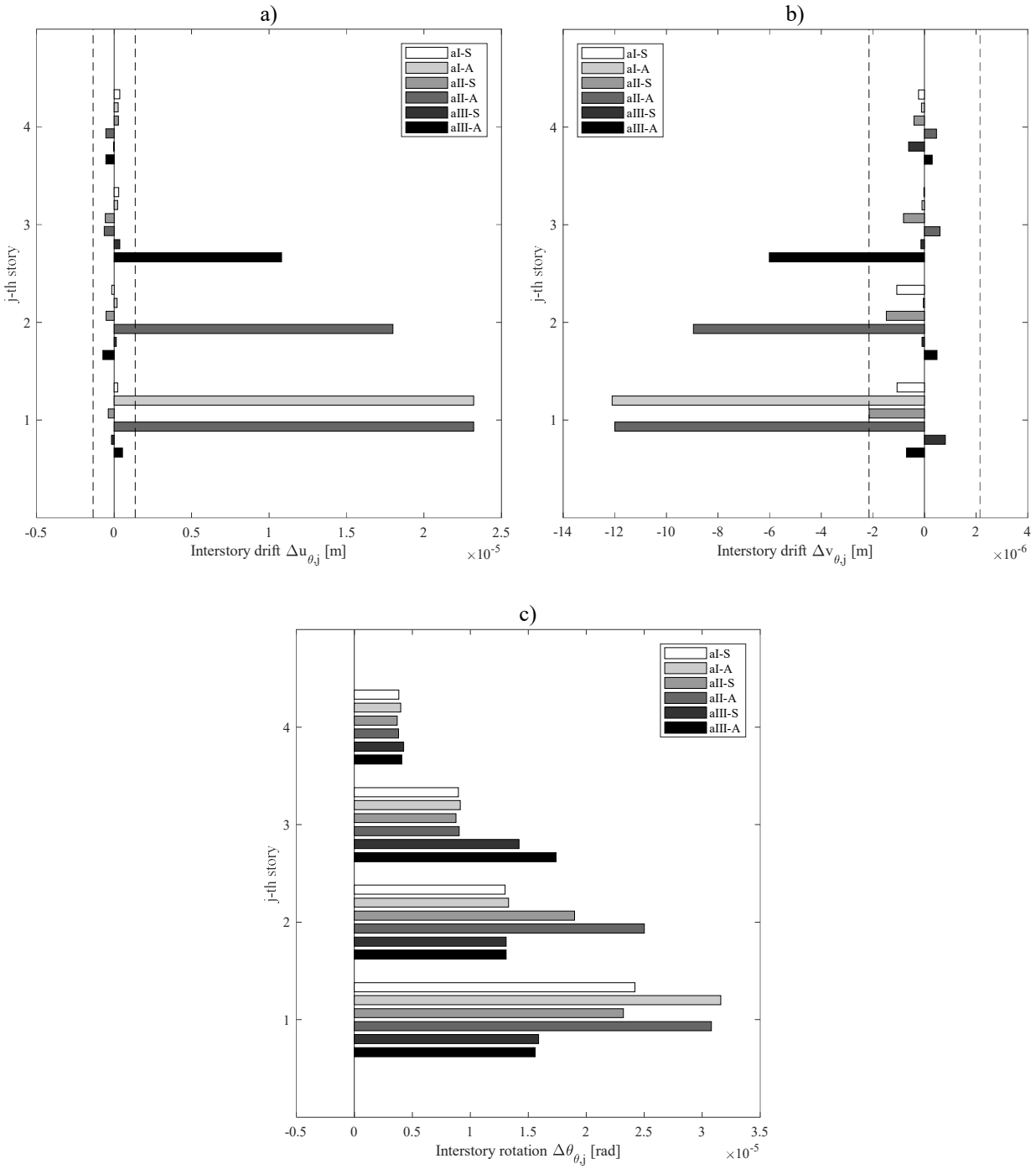

Figure 5. Interstory movements of the modal flexibility-based deflections due to the load $\boldsymbol{p_\theta}$ composed by unitary torques (numerical simulation): a) interstory drifts in *x* direction; b) interstory drifts in *y* direction; c) interstory rotations.

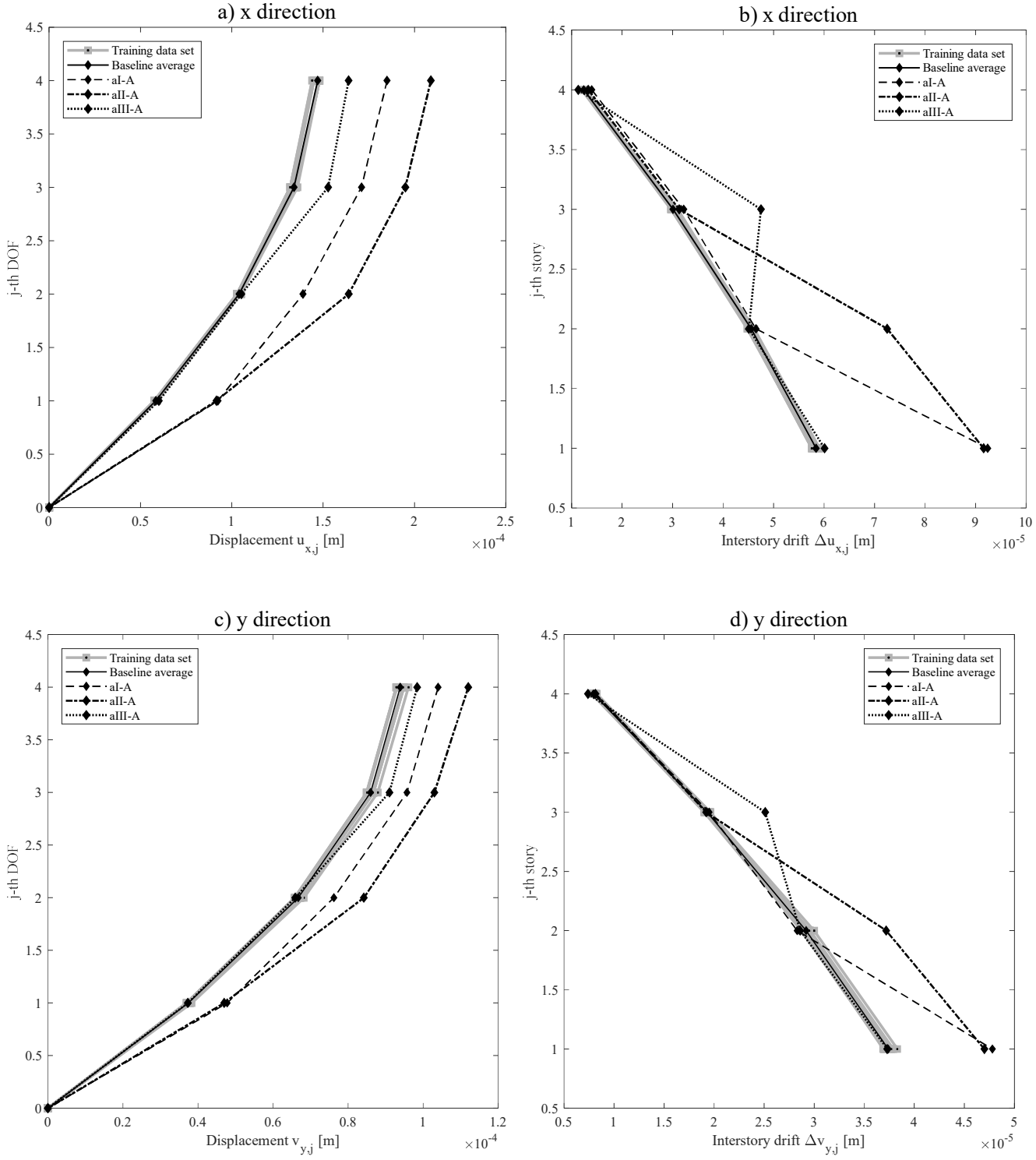

Figure 6. Modal flexibility-based deflections due to the UL+T loads for the baseline structure and for the plan-asymmetric damaged configurations (numerical simulation). Parameters: a,c) displacements; b,d) interstory drifts. Directions: a,b) analysis in *x* direction; c,d) analysis in *y* direction.

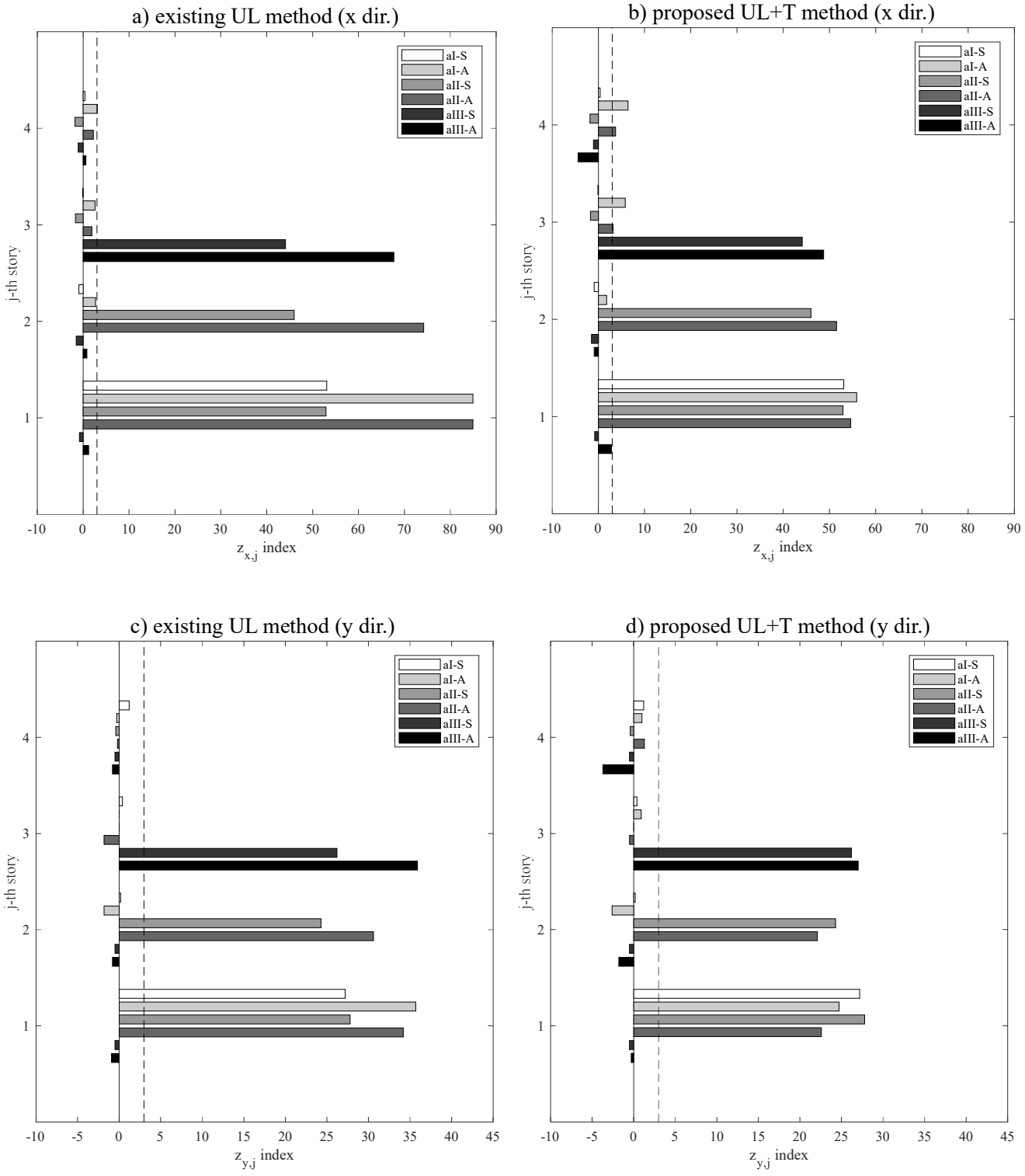

Figure 7. Damage detection/localization on the frame structure (numerical simulation). Methods: a,c) existing UL method; b,d) proposed UL+T method. Directions: a,b) analysis in *x* direction; c,d) analysis in *y* direction.

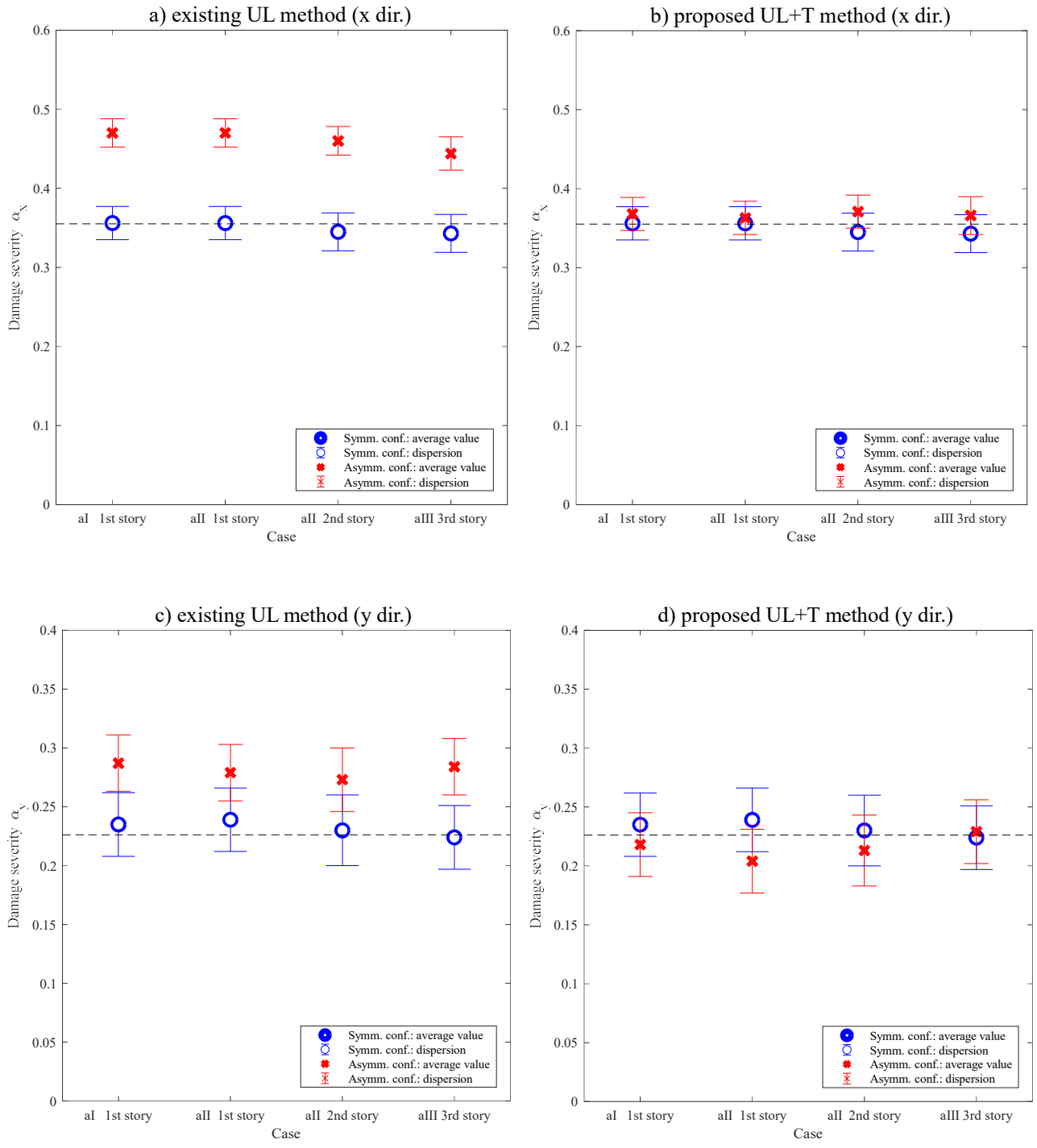

Figure 8. Damage quantification on the frame structure (numerical simulation) (average values of the damage severity ± 3 standard deviations). Methods: a,c) existing UL method; b,d) proposed UL+T method. Directions: a,b) analysis in *x* direction; c,d) analysis in *y* direction. Dashed line: reference value of damage severity evaluated from the analytical model.

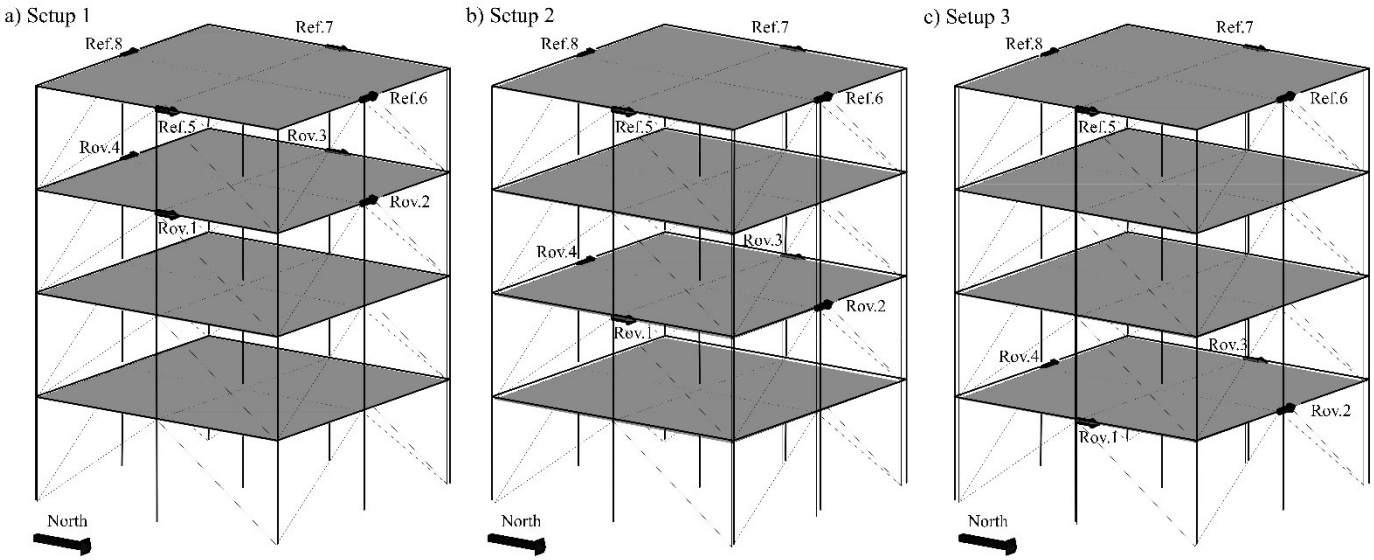

Figure 9. Setups and sensor layouts used in the numerical simulation of the multi-setup OMA test (Ref. = reference sensor; Rov. = roving sensor): a) setup 1; b) setup 2; c) setup 3.

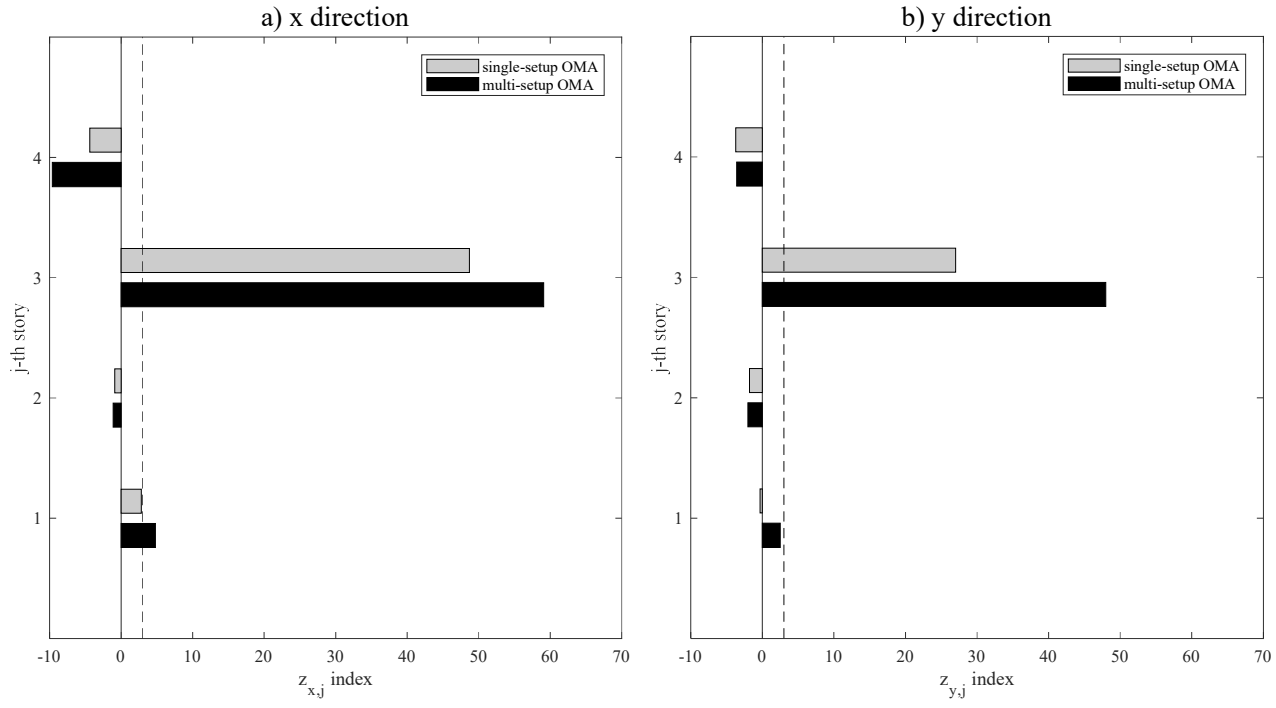

Figure 10. Damage detection/localization using the proposed UL+T method for the multi-setup OMA test on configuration aIII-A of the frame structure (numerical simulation and comparison w.r.t. results of single-setup OMA test): a) analysis in *x* direction; b) analysis in *y* direction.

Figure 11. Steel frame structure used for the experimental validation (EERF laboratory, UBC) [13].

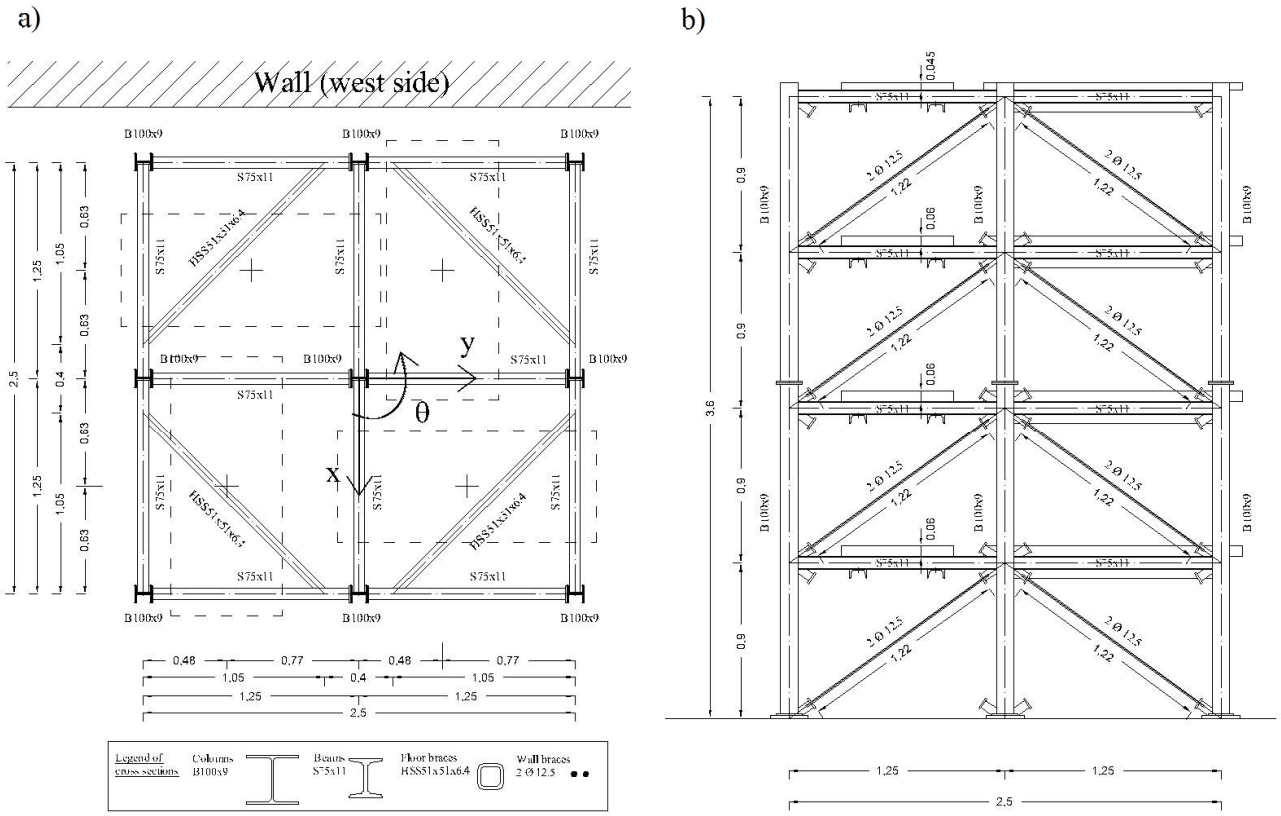

Figure 12. Geometry of the steel frame structure tested under ambient vibrations (dimensions in m): a) plan view; b) lateral view of the south face.

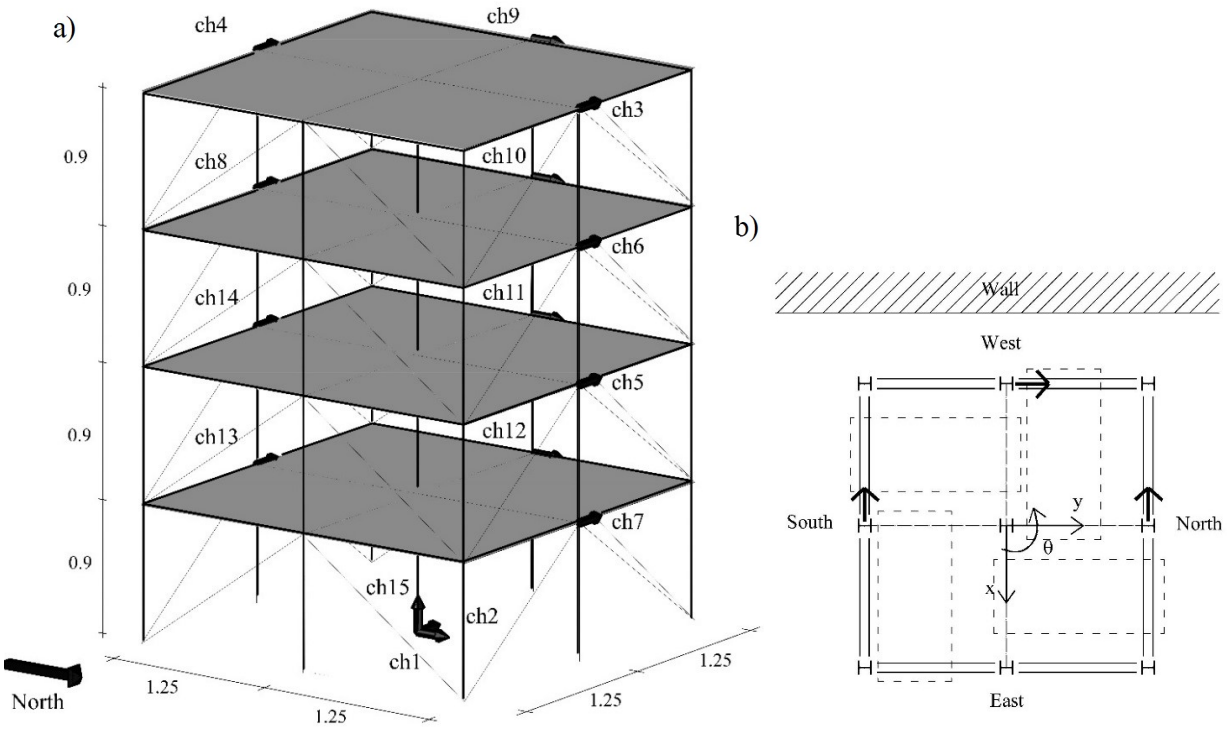

Figure 13. Layout of the sensors used in the ambient vibration tests (dimensions in m): a) 3D view; b) plan view.

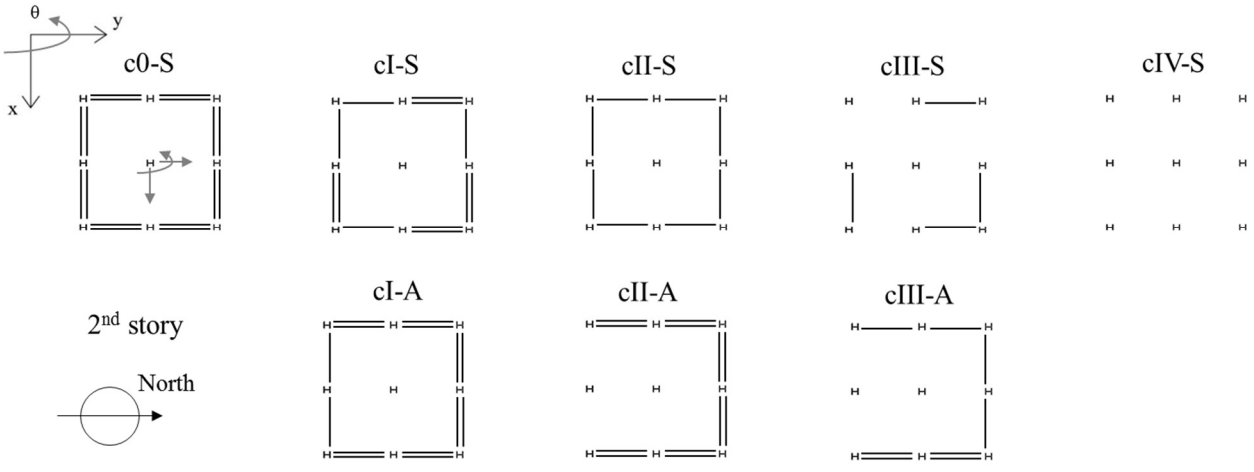

Figure 14. Schematic plan view of the 2nd story of the configurations considered in the ambient vibration tests.

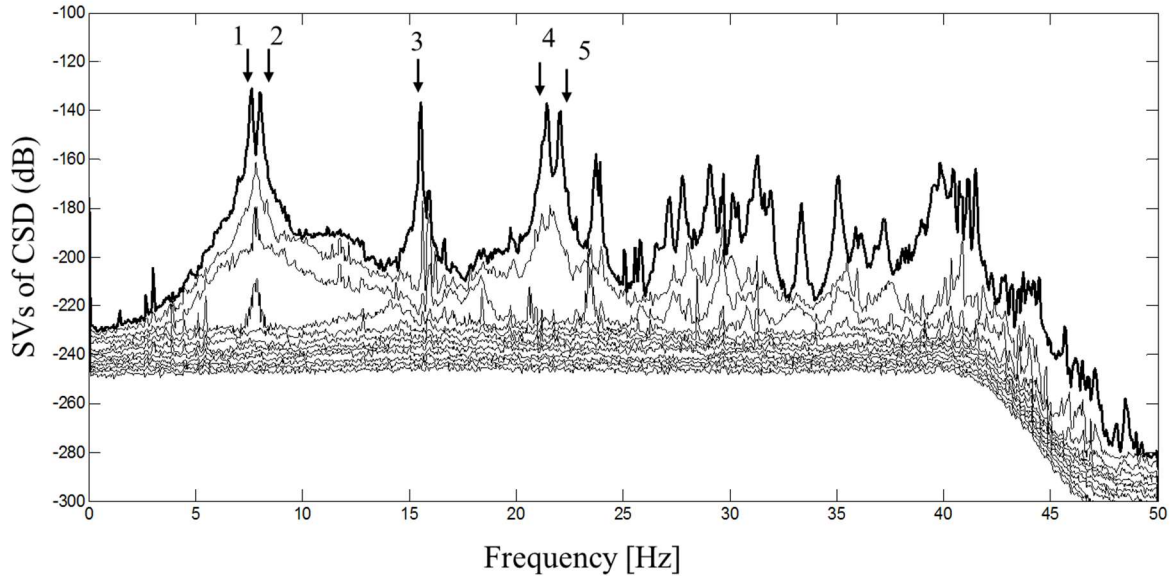

Figure 15. Singular values (SV) computed from the cross spectral density (CSD) matrix – configuration c0-S (AV tests).

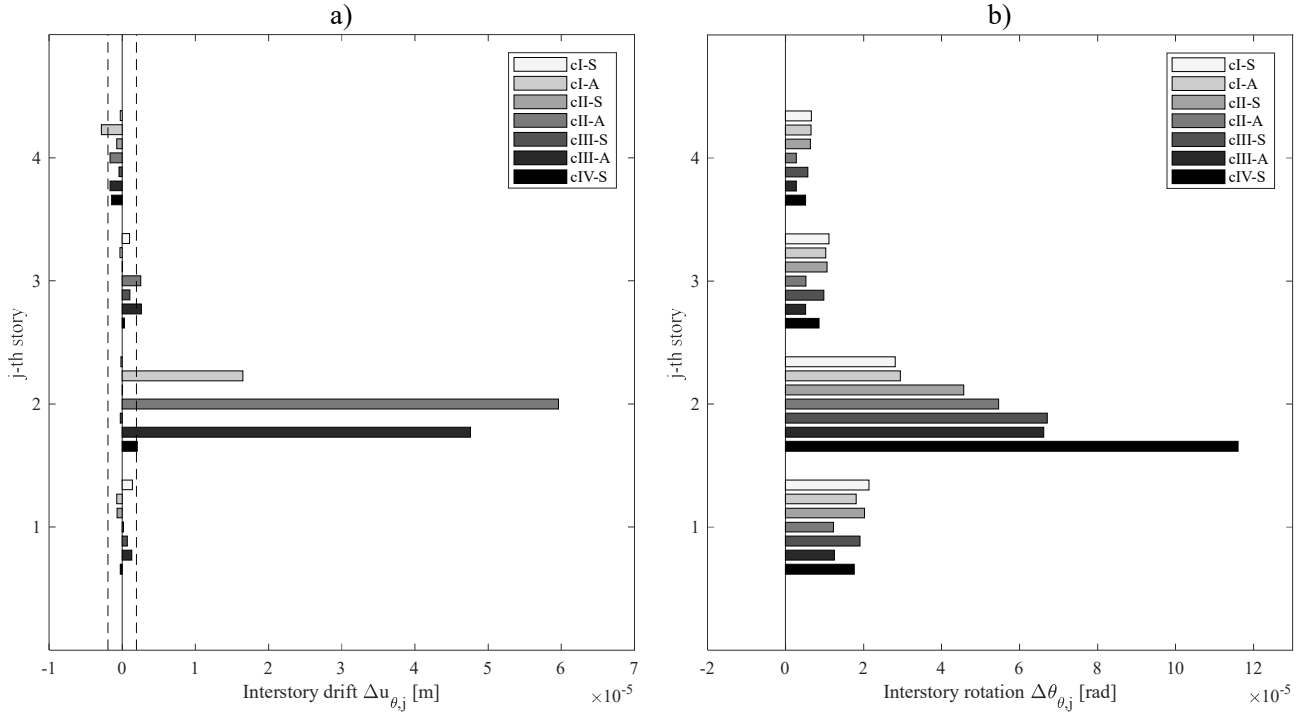

Figure 16. Interstory movements of the modal flexibility-based deflections due to the load $\boldsymbol{p_\theta}$ composed by unitary torques (AV tests): a) interstory drifts in x direction; b) interstory rotations.

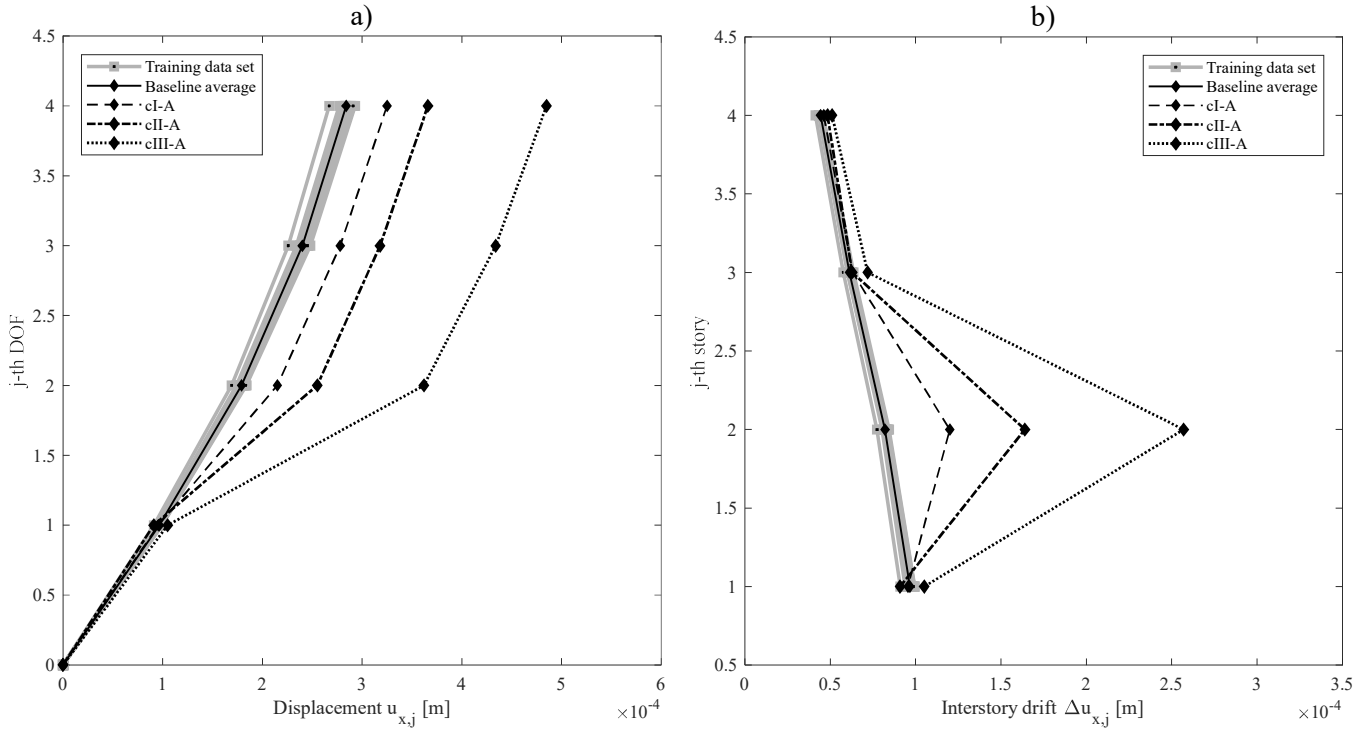

Figure 17. Modal flexibility-based deflections due to the ULx+T load for the baseline structure and for the plan-asymmetric damaged configurations (components in *x* direction, AV tests). Parameters: a) displacements; b) interstory drifts.

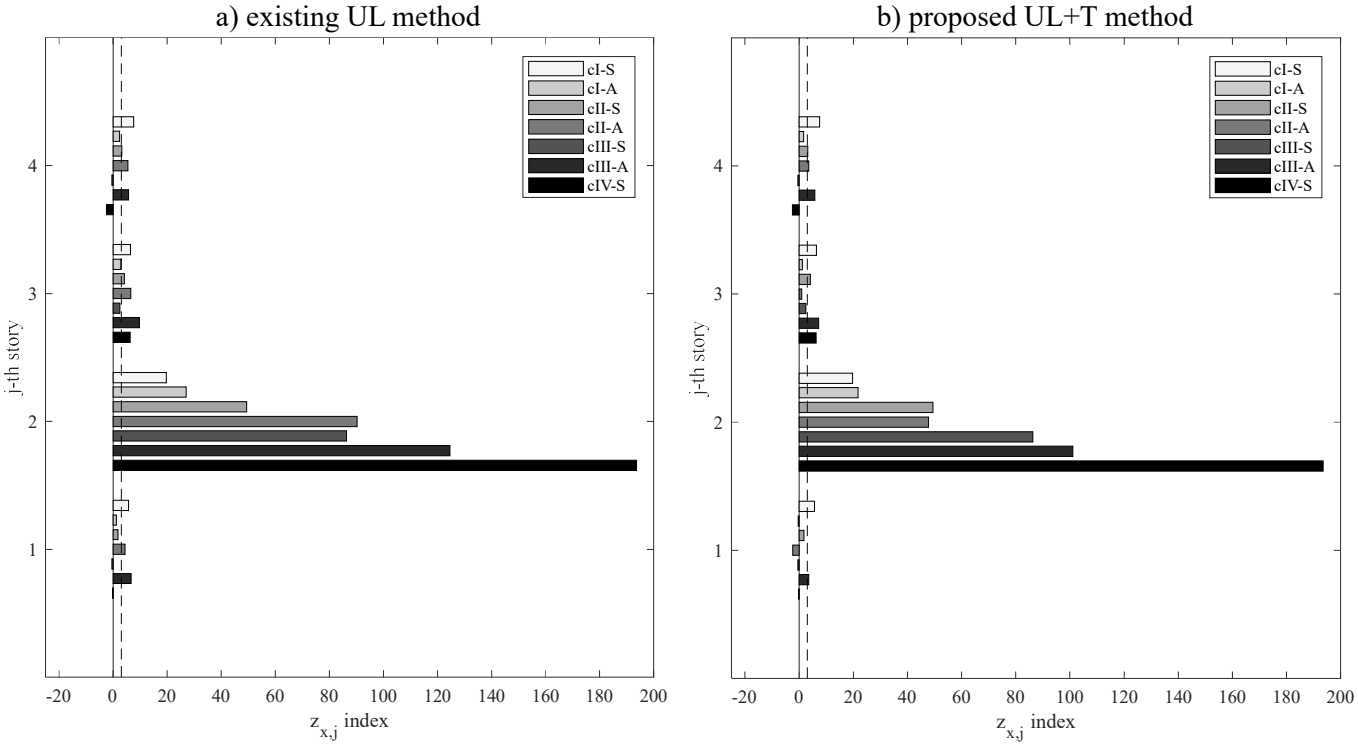

Figure 18. Damage detection/localization on the 4-story steel frame structure (analysis in *x* direction, AV tests): a) existing UL method; b) proposed UL+T method.

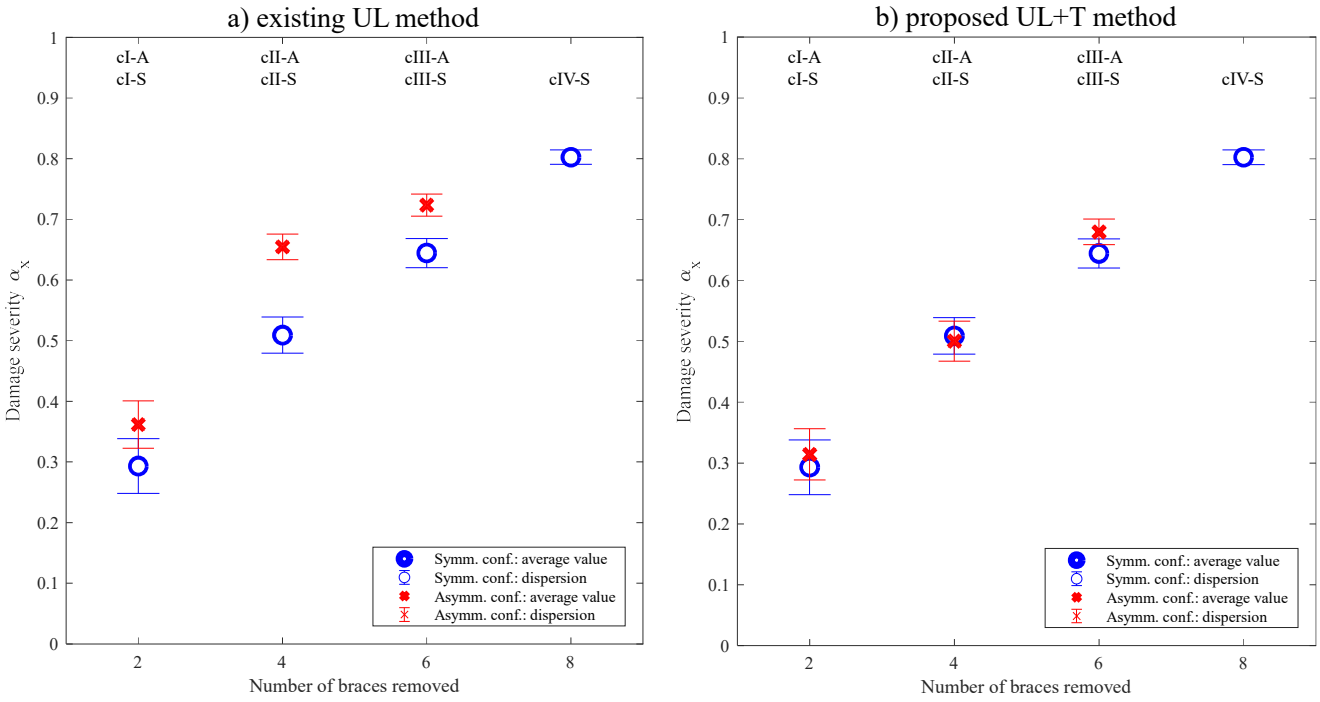

Figure 19. Damage quantification on the 4-story steel frame structure (analysis in *x* direction, AV tests) (average values of the damage severity ± 3 standard deviations): a) existing UL method; b) proposed UL+T method.

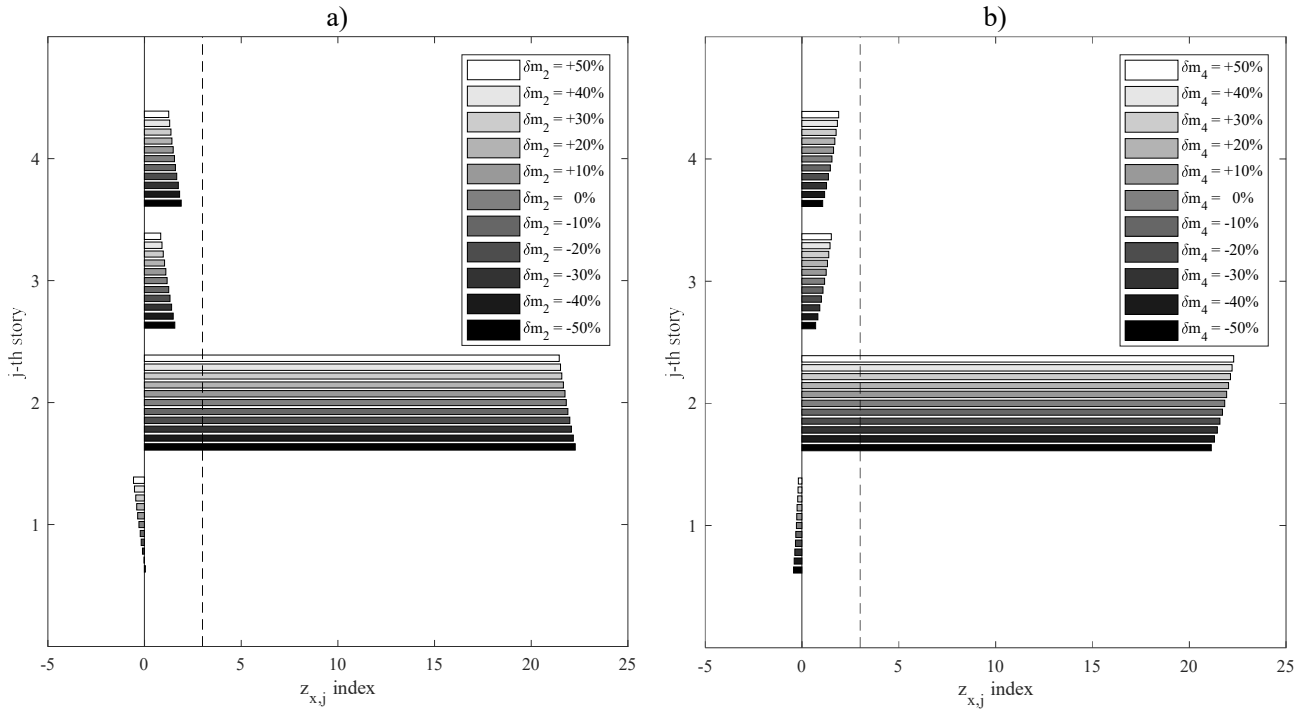

Figure 20. Effect of potential errors in mass matrix estimation on the z index for damage detection/localization for configuration cI-A (proposed method; ambient vibration tests): a) mass perturbations at 2nd story; b) mass perturbations at 4th story.